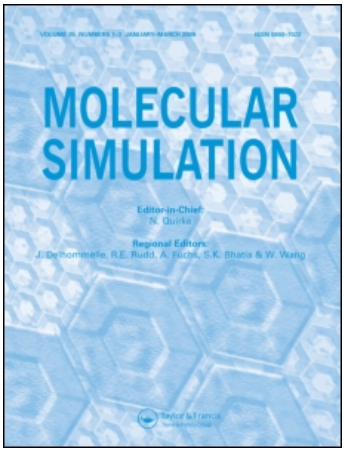

Molecular Simulation
Publication details, including instructions for authors and subscription information:
http://www.informaworld.com/smpp/title~content=t713644482

Temperature-and-density-scaling Monte Carlo: isothermal-isobaric thermodynamics of Lennard-Jonesium

John P. Valleau[a]
[a] Chemical Physics Theory Group, Department of Chemistry, University of Toronto, Toronto, Ontario, Canada

To cite this Article Valleau, John P.(2005) 'Temperature-and-density-scaling Monte Carlo: isothermal-isobaric thermodynamics of Lennard-Jonesium', Molecular Simulation, 31: 4, 255 — 275
To link to this Article: DOI: 10.1080/08927020500036133
URL: http://dx.doi.org/10.1080/08927020500036133

Molecular Simulation, Vol. 31, No. 4, 15 April 2005, 255–275

Taylor & Francis
Taylor & Francis Group

Temperature-and-density-scaling Monte Carlo: isothermal–isobaric thermodynamics of Lennard-Jonesium

JOHN P. VALLEAU*

Chemical Physics Theory Group, Department of Chemistry, University of Toronto, Toronto, Ontario, Canada M5S 3H6

(Received September 2004; in final form September 2004)

In the "thermodynamic limit" thermodynamic quantities have the same values regardless of the ensemble in which they may be generated, but this is by no means the case for the small systems to which simulations are restricted. A preceding paper ["Temperature-and-density-scaling Monte Carlo: methodology and the canonical thermodynamics of Lennard-Jonesium" *Molecular Simulation* 2005] discussed temperature-and-density-scaling Monte Carlo, and used the results of one such run to generate accurate thermodynamic data for Lennard-Jones fluids in the canonical ensemble, continuously throughout a substantial region of temperature and density. This paper demonstrates how the *same* data can instead be used to generate the accurate thermodynamics of the system within the isothermal–isobaric ensemble, now continuously throughout a substantial region of temperature and pressure. This evidently constitutes an alternative method of generating precise isothermal–isobaric thermodynamics, one which may often be particularly efficient. Results in the canonical and isothermal–isobaric ensembles are compared in some detail; the discrepancy of behaviour in the coexistence and critical regions is of course striking; nevertheless the two ensembles bracket the limiting coexistence behaviour rather closely. Some preliminary analysis of the critical behaviour is carried out, but a fully-detailed finite-size scaling analysis is deferred.

Keywords: Monte Carlo; Thermodynamic scaling; Equation of state; Coexistence

1. Introduction

In the preceding paper [1] data obtained using "temperature-and-density-scaling" Monte Carlo (TDSMC) were used to generate the thermodynamics of Lennard-Jonesium in the *canonical ensemble*. In this way precise canonical free energy and the other canonical properties can be obtained, essentially continuously, throughout a substantial range of temperature and density, using only a small number of TDSMC runs (e.g. only *one* run in the cited example). It is the purpose of this paper to demonstrate that the *same* TDSMC data can as well be analysed to obtain the thermodynamics of the finite system within the *isothermal–isobaric ensemble*, over the same temperature range and a substantial pressure range; we generate such results.

In the "thermodynamic limit" the various ensembles employed in statistical mechanics must lead to identical equations of state between thermodynamic properties. This limiting behaviour reflects the fact that the relative fluctuations of thermodynamic variables vanish in the large-system limit.

For systems of finite size one can define a "pseudo-thermodynamics" within a particular ensemble, generated by applying the familiar relations between the statistical and thermodynamic quantities, starting from the corresponding partition function; this is what is ordinarily done in interpreting simulation data. However the resulting equations of state are no longer strictly independent of the ensemble in which they are generated; this is because relative fluctuations need no longer vanish, and in the different ensembles different properties are allowed to fluctuate. It is of interest to examine this ensemble-dependence of the apparent thermodynamics in small systems, as we do in this article by comparing the canonical and isothermal–isobaric cases. It is particularly relevant in interpreting data from Monte Carlo or molecular dynamics simulations, which necessarily refer to quite small systems; simulation results obtained in different ensembles have often been compared without taking into account discrepancies which may be intrinsic to the ensembles, but with the improved precision now possible this can no longer be regarded as acceptable.

*Corresponding author. Email: jvalleau@chem.utoronto.ca

Molecular Simulation
ISSN 0892-7022 print/ISSN 1029-0435 online © 2005 Taylor & Francis Group Ltd
http://www.tandf.co.uk/journals
DOI: 10.1080/08927020500036133

These discrepancies are likely to be particularly important in attempting to study phase transitions and criticality, due to the large fluctuations then to be expected; they can in fact be quite striking in the parts of the phase diagram describing such phenomena. As a result, some ensembles may be superior to others for such studies, and the appropriate analyses will depend on the ensemble employed.

It would be useful, then, to obtain comprehensive data for a model system in each of several ensembles, and to compare their behaviours. To do this using conventional simulation techniques would however be tedious and rather difficult to achieve. In the preceding paper [1] we described the use of "thermodynamic scaling" to generate precise and essentially continuous data on the canonical Helmholtz free energy throughout a substantial pre-selected region of temperature and density—a region including the upper part of the liquid–gas coexistence curve. This was done for systems with various fixed numbers of particles N, using a *single* Monte Carlo run of the type called TDSMC for each N. In that paper these data were used to generate the pseudo-thermodynamics in the *canonical* ensemble. This choice of ensemble within which to analyse the data seemed natural in view of fact that the basic independent variables of the canonical ensemble, (N,ρ,T)—namely the number of particles N, the density $\rho \equiv N/V$ (where V is the volume) and the temperature T—are also the variables used to define the states within TDSMC. What is interesting, however, is that the *same* TDSMC data can equally be used to generate, instead, the thermodynamics within the II ensemble, in which the states are specified by the values of (N,p,T), where p is the pressure, as demonstrated below. Since the *same* (good) data are used to generate both sets of results, we are able to examine the ensemble dependence itself in some detail, without confusions due to discrepant errors in simulation data.

In what follows this programme is carried out, using the Lennard-Jones system as an example. In the following section we discuss how the isothermal–isobaric (II) results can be generated from TDSMC data. We then obtain much new II data for this system, including the Gibbs free energy (Section 3) and both first-order and second-order thermodynamic functions (Section 4); we then examine the liquid–gas coexistence in some detail (Section 5). The data is appropriate for examining the critical properties associated with this coexistence: we do some preliminary analysis concerning this (but a fully detailed finite-size scaling analysis is deferred to a later publication).

2. Isothermal–isobaric analysis of TDSMC data

In the II ensemble the states of a one-component system are defined by the trio of values (N,p,T). The corresponding II partition function Γ may be written*

$$\Gamma(N,p,T) = \int_0^\infty \mathrm{d}V \frac{1}{\tilde{V}} e^{-\beta pV} Q(N,V,T), \qquad (1)$$

where $\beta = 1/k_B T$ (with k_B Boltzmann's constant) and $Q(N,V,T)$ is the canonical partition function; the factor $\tilde{V}$ has the dimensions of volume, to render Γ dimensionless. There have actually been several suggestions as to the functional form of $\tilde{V}$. Hill [2] (and more recently Attard [3]) proposed that it should be taken as constant, but other forms have been proposed based on various arguments, for example that $\tilde{V} = 1/\beta p$ (Sack [4]), $\tilde{V} = V$ (Attard [5]), etc. [6–8]. It should be noted that properties evaluated under the various choices of $\tilde{V}$ must all converge in the thermodynamic limit (since the volume distribution then becomes perfectly sharp in any case); however that is not the case for finite systems (such as those used in simulations). This is not the place to re-evaluate the arguments for particular choices of $\tilde{V}$. Instead we adopt in what follows the point of view of Hill, that $\tilde{V}$ be taken as a *constant* volume; its value is then arbitrary, in the sense that it will appear in no estimated observable of a fluid property, and we assign to it unit volume. This choice is attractive in that it has been the basis for nearly all simulation estimates within the II ensemble.

It is important to point out, meanwhile, that the point of the present work, namely that the TDSMC data can be used to generate the II pseudothermodynamics, is equally true for *any* of the proposed choices for the form of $\tilde{V}$: one gets the results (which will depend on the choice, since the systems are finite) with equal ease in any case.

Using the relation between $Q(N,V,T)$ and the canonical Helmholtz free energy $A^{\mathrm{Can}}(N,V,T)$ (and setting $\tilde{V} = 1$), we may re-write equation (1) in the form

$$\Gamma(N,p,T) = \int_0^\infty \mathrm{d}V e^{-\beta pV} e^{-\beta A^{\mathrm{Can}}(N,V,T)}, \qquad (2)$$

and we recall that the II Gibbs free energy $G^{\mathrm{II}}(N,p,T)$ is given by

$$\beta G^{\mathrm{II}}(N,p,T) = -\log \Gamma(N,p,T), \qquad (3)$$

where, (here and elsewhere) the superscript "II" identifies the II ensemble. It is then clear how to proceed, because we have already determined from the TDSMC simulation [1] the *relative* canonical Helmholtz free energy

$$\Delta(\beta A^{\mathrm{Can}}(N,V,T)) \equiv \beta A^{\mathrm{Can}}(N,V,T) - \beta_{\mathrm{ref}} A^{\mathrm{Can}}(N,V_{\mathrm{ref}},T_{\mathrm{ref}}), \qquad (4)$$

relative to a reference state $(N, V_{\mathrm{ref}}, T_{\mathrm{ref}})$, over a wide range of V and T (for a few values of N). This evidently enables us to generate in turn relative Gibbs free energies in the II ensemble over a wide range of pressure and temperature, relative to some arbitrary II reference state (N, p_0, T_0),

*The symbol Δ is more frequently used (cf. [2]) for this partition function; we have instead adopted Γ, because the symbol Δ is required in what follows, for a different purpose.

according to

$$\Delta(\beta G^{\mathrm{II}}(N,p,T)) \equiv \beta G^{\mathrm{II}}(N,p,T) - \beta_0 G^{\mathrm{II}}(N,p_0,T_0) = -\log\left(\frac{\Gamma(N,p,T)}{\Gamma(N,p_0,T_0)}\right), \quad (5)$$

where

$$\frac{\Gamma(N,p,T)}{\Gamma(N,p_0,T_0)} = \frac{\int_0^\infty \mathrm{d}V e^{-\beta pV} e^{-\Delta(\beta A^{\mathrm{Can}}(N,V,T))}}{\int_0^\infty \mathrm{d}V e^{-\beta_0 p_0 V} e^{-\Delta(\beta_0 A^{\mathrm{Can}}(N,V,T_0))}}, \quad (6)$$

(since the terms associated with the free energy of the canonical reference state cancel out of this ratio). The integrals appearing in equation (6) are readily evaluated (up to a constant factor which disappears from the ratios) from the TDSMC data, as described below.

When it comes to generating the other thermodynamic properties within the II ensemble, more than one path is available. One route follows from noting that, having determined the relative reduced Gibbs free energy $\Delta(\beta G^{\mathrm{II}}(N,\ p,\ T))$ as a function of pressure and temperature, using equations (5) and (6), the other thermodynamic functions can be obtained by differentiating this quantity with respect to these variables, in the usual way. Alternatively, where such properties can be written in the form of ensemble averages, they can be generated more directly, in the form

$$\langle X\rangle^{\mathrm{II}}_{N,p,T} = \frac{\int_0^\infty \mathrm{d}V X(N,V,T) e^{-\beta pV} e^{-\Delta(\beta A^{\mathrm{Can}}(N,V,T))}}{\int_0^\infty \mathrm{d}V e^{-\beta pV} e^{-\Delta(\beta A^{\mathrm{Can}}(N,V,T))}}, \quad (7)$$

where $X(N,V,T)$ might be either an explicit function of its variables or a canonical expectation value (or a linear combination of these). For example, setting $X = V/N$ we obtain the mean specific volume

$$\langle v\rangle^{\mathrm{II}} = \langle V/N\rangle^{\mathrm{II}}_{N,p,T} = \frac{\int_0^\infty \mathrm{d}V (V/N) e^{-\beta pV} e^{-\Delta(\beta A^{\mathrm{Can}})}}{\int_0^\infty \mathrm{d}V e^{-\beta pV} e^{-\Delta(\beta A^{\mathrm{Can}})}}, \quad (8)$$

or, setting $X = \langle E\rangle^{\mathrm{Can}}_{N,V,T}$, the mean II internal energy

$$\langle E\rangle^{\mathrm{II}}_{N,p,T} = \frac{\int_0^\infty \mathrm{d}V e^{-\beta pV} \langle E\rangle^{\mathrm{Can}}_{N,V,T} e^{-\Delta(\beta A^{\mathrm{Can}})}}{\int_0^\infty \mathrm{d}V e^{-\beta pV} e^{-\Delta(\beta A^{\mathrm{Can}})}}, \quad (9)$$

where the averages are labelled as to their ensembles and state variables. In examining finite systems, both approaches have been used with the present data and their consistency confirmed.

We will be examining a system of Lennard-Jones particles, for which the pair potential $\phi(r)$ between particles separated by a distance r is determined by the parameters ε, σ, according to

$$\phi(r) = 4\varepsilon\left(\left(\frac{\sigma}{r}\right)^{12} - \left(\frac{\sigma}{r}\right)^{6}\right). \quad (10)$$

(In practice the model used also involves a spherical cutoff at half the length of the cubic box involved in the computation, and a tail correction for larger separations; the details are described in ref. [1]). It is convenient to use the parameters ε and σ to define the reduced pressure $p* \equiv p\sigma^3/\varepsilon$, the reduced temperature $T* \equiv k_B T/\varepsilon$ (where k_B is Boltzmann's constant), and the reduced density $\rho* \equiv N\sigma^3/V$. We thus also have the reduced *specific* volume $v* \equiv V/N\sigma^3 \equiv 1/\int*$ and a reduced isothermal compressibility $\kappa_T^* \equiv \kappa_T\varepsilon/\sigma^3$, while $\beta pV \equiv Np*v*/T*$.

Evidently, to evaluate integrals like those in equations (6)–(9), we need the relative canonical Helmholtz free energy as a function of density and temperature. Data on this quantity was originally extracted during the TDSMC run, on a grid with intervals of 0.01 in both $\rho*$ and $T*$. These intervals are not sufficiently fine for the present purpose, however, so interpolation is required. This could be done locally, but as discussed in the preceding paper [1], a convenient way of interpolating those data was to fit to the relative canonical excess Helmholtz free energy a global many-parameter algebraic function. We demonstrated that an excellent fit, within the statistical uncertainty for all 901 state points, could be obtained as a ratio of double power series in density and temperature; the parameters for such a fit (involving 59 fitting constants) for $N = 500$ were given (see table 2 of that paper [1]); similar fits are available for the smaller systems studied. Such a fit is here referred to as an "A-fit". These A-fits were used for evaluating the integrals of equations (6)–(9), and thus the isothermal–isobaric results in this paper. Likewise, any required *canonical* averages (such as that appearing in equation (9)), are readily estimated algebraically using this fitted function [1].

In principle, the integrals in equations (6)–(9) could be evaluated algebraically from the A-fits, but this is actually completely impracticable. Instead, the integrals over volume were approximated by sums; in practice it was convenient to sum over densities, rather than volumes, after introducing the appropriate Jacobian:

$$\int \mathrm{d}V(\cdots) \simeq \sum_k \frac{-N\delta\rho_k}{{\rho_k}^2}(\cdots). \quad (11)$$

This can be done on an arbitrarily fine density interval $\delta\rho_k$ by using the algebraic A-fits to evaluate each term of the sums; the density interval must be sufficiently fine to ensure an accurate approximation of the integral, and this was tested.

In principle, the sums include all possible densities, from zero to infinity; in practice, at a given temperature and pressure, only a limited range of densities contributes. We are able to generate accurate II results for those pressures and temperatures for which the TDSMC computation provides accurate free energies throughout the relevant range of densities. That is, that range must lie essentially within the $\rho*$-range of the TDSMC computation, which in the present case extended from 0.08 to 0.60. This consideration prescribes the range of pressures over which we can generate II thermodynamic results

(for each temperature within the target range of the TDSMC run) as we now describe. The "A-fit" to $\Delta(\beta A^{\mathrm{Can,ex}})$ used in the evaluation interpolates the TDSMC results, but presumably it will extrapolate successfully to densities very slightly above or very slightly below the measured TDSMC density range. So by extending the density sum very slightly beyond that range, we can estimate what contribution to the sum, if any, arises from densities just above or just below the TDSMC range. The minimum usable pressure was chosen to ensure that not more than 2% of the partition function arose from densities $\rho*$ less than 0.08; this small contribution from extrapolated values then arises from densities within only a few per cent of 0.08, where one would confidently expect satisfactory extrapolation. Similarly, to define the high-pressure limit, not more than 2% of the sum arose from densities greater than 0.60, and a similar remark applies regarding the range of such an extrapolation. This seems fairly conservative; we could certainly find no evidence that the criterion introduced any error at the lower or upper pressure limits thus defined. These upper and lower limits (of the pressure ranges for which we expect to be able to estimate II properties from the available TDSMC data) are displayed, for each system size, in figure 1. The accessible pressure ranges are very small at low temperatures; that is because the chosen TDSMC density range was only very little larger than the coexistence density gap. (In particular, as we see in the figure, *no* reliable II data based on our TDSMC data [1] is available below $T* = 1.24$ for the very small sytem $N = 72$, because the density fluctuations are then so large that they escape the TDSMC density range at *any* pressure). We should reiterate that the above criterion is simply to define the accessible pressure range at each temperature, given the particular TDSMC data at hand; for almost all the states for which thermodynamic data is presented—all but those at the extreme pressure limits so defined—the relevant ranges of density lie in fact well within the available TDSMC range. The annoying feature of the limited pressure range available using the present data is that it turns out to limit the temperature range over which coexistence data is available for the smaller systems (N of 72 and 256), though luckily not for $N = 500$. This limitation could have been avoided very easily, simply by including a slightly larger density range in the TDSMC computation (had one only had one's wits about one sufficiently to have anticipated the present application of the TDSMC data!).

Within the accessible ranges, the integrals can be evaluated and properties thus evaluated for any state ($p*$, $T*$). In practice, the thermodynamic quantities were evaluated for a fine grid of states, at intervals of 0.001 in reduced temperature (171 temperatures in all) and 0.0001 in reduced pressure. (The small pressure intervals were useful in view of the very strong dependence of some properties on pressure in the "phase separation" region).

As mentioned above, thermodynamic functions may be calculated either as direct averages (equations (7)–(9)) or by taking temperature or pressure derivatives of the Gibbs free energy or of derived properties. Where numerical differentiation was employed it used five-point estimates of the first or second order derivatives [9], based on the intervals noted above, namely 0.001 in $T*$ and 0.0001 in $p*$.

A problem associated with the use of the algebraic fits (A-fits) to the TDSMC data, in deriving II results, is the difficulty of then generating detailed error estimates for the resulting II thermodynamic properties. In the case of the canonical ensemble [1] analysis of the raw free energy data collected allowed explicit point-by-point error estimates. The A-fits gave everywhere "fitted" free

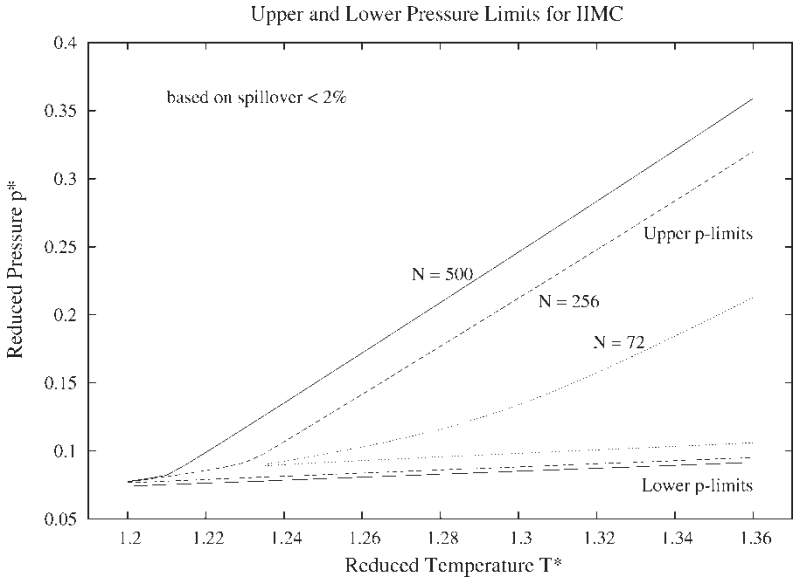

Figure 1. Ranges of pressure available for calculation of isothermal–isobaric thermodynamics, using the particular set of TDSMC data available. The figure gives the upper and lower pressure limits as a function of temperature, for each system size N. (The density range of the TDSMC data was the same, $0.08 < \rho* < 0.60$, for each size; the wider density distribution for smaller systems restricts the corresponding pressure range).

energies well within those estimated errors, in fact usually deviating by much less than the estimated standard deviation from the raw estimates (cf. figure 6 of [1]). This is an aspect of the data-smoothing inherent in the fitting procedure, and implies that the A-fits are giving results more precise than the raw data (and particularly that derivatives of the free energy calculated from the fits will be more precise than that from point-by-point numerical differentiation of the original data). In addition, the II results involve further averaging over volume, as we have seen, which will also reduce the random errors. These facts are all very encouraging with respect to the precision of the II estimates; the problem lies in the difficulty of making these remarks on precision quantitative. Instead, we have been satisfied with setting some bounds and/or making plausible guesstimates of the error bounds, as discussed with respect to individual properties in the sections of the paper below.

The following sections examine the resulting Gibbs free energies (Section 3), other thermodynamic properties in the II ensemble (Section 4), and the liquid–gas coexistence (Section 5) (including some remarks on critical behaviour). In each case the details required in exploiting the above formulas (5)–(7) are described, and the II thermodynamics is frequently compared with the canonical.

3. The Gibbs free energy

The basic thermodynamic potential function in the II ensemble is the Gibbs free energy G^{II} or the corresponding "chemical potential" $\mu^{\mathrm{II}} = G^{\mathrm{II}}/N$. The dimensionless relative II relative chemical potential $\Delta(\beta\mu^{\mathrm{II}})$, at a given state ($N$, $p*$, $T*$), relative to a reference state, is easy to generate from (5),(6) after replacing the integral by a sum (11) and introducing $\Delta(\beta A^{\mathrm{Can}})$, obtained by adding the *ideal* part of the relative canonical free energy to the *excess* part described by the "A-fit". This can evidently be done using an arbitrarily fine grid of densities; in practice we report results based on 581 equal intervals covering very slightly more than the range (0.08–0.60) of the TDSMC densities. (These intervals are sufficiently small that decreasing them further makes no observable difference in the resulting II properties). The reported Gibbs free energy results are for the difference of the $\beta G^{\mathrm{II}}/N \equiv \beta\mu^{\mathrm{II}}$ from that in an (arbitrarily chosen) reference state (N, p_0^*, T_0^*) with $p_0^* = 0.130$ and $T_0^* = 1.30$ (cf. (5)).

Results for $\Delta(\beta\mu^{\mathrm{II}})$ (and for the other thermodynamic properties as reported in the following section) were calculated within the accessible pressure ranges for temperatures $T*$ from 1.20 to 1.36, at intervals of 0.001. The accessible pressure ranges depended on the temperatures, as explained; within those ranges, results at each temperature were calculated at intervals of 0.0001 in $p*$. (This fine pressure grid was used to ensure faithful rendering of those properties exhibiting rather sharp variation with pressure in the vicinity of phase coexistence or the critical region). In view of the fine grid of II states for which properties were evaluated, the reported results (not only for chemical potential, but for all the thermodynamic quantities) are everywhere plotted as lines joining adjacent states, e.g. those along an isotherm; of course in view of the very fine grid of states the plots have the superficial appearance of smooth continuous curves.

Figure 2 shows the relative reduced chemical potential for $N = 500$ particles as a function of pressure for a few of the 171 temperatures studied, namely at intervals of 0.01 in $T*$ from $T* = 1.20$ to 1.36. These curves have everywhere a negative curvature, which corresponds to the thermodynamic stability condition of positive

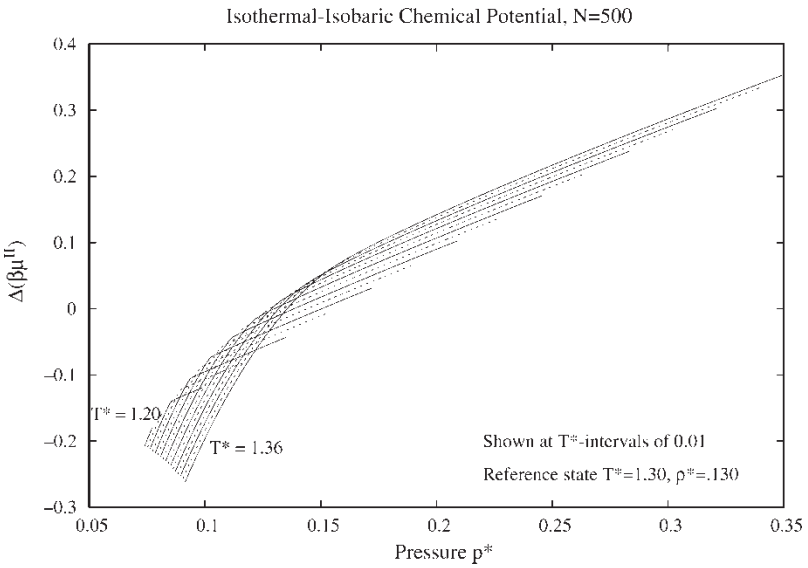

Figure 2. Some isotherms of II relative chemical potential $\Delta(\beta\mu^{\mathrm{II}})$ for $N = 500$, relative to the reference state $T* = 1.30$, $\rho* = 0.130$.

compressibility. The slopes change from large to small as the pressure increases, which corresponds to the change from low density to high. At low temperatures this change is very sharp, reflecting a first-order phase change: in the thermodynamic limit there would of course be an actual 'kink'—i.e. a discontinuity of the slope—occurring at the vapour pressure. The temperature dependence changes sign as one passes through the transition region: this corresponds to the change of enthalpy during condensation of the gas to liquid, as we examine in more detail below.

We have mentioned the difficulty of carrying out detailed error analysis for these data. In the case of the relative Gibbs free energy (see (5),(6)) errors arise only through those of $\Delta(\beta A^{\mathrm{Can}})$. For the most widely separated II states covered, the differences of mean density are about 0.47, and the corresponding standard deviation of the raw values of $\Delta(\beta A^{\mathrm{Can}})/N$ will be about 0.0005. We may regard this as a very conservative upper bound for the errors of $\Delta(\beta\mu^{\mathrm{II}})$, because (i)in forming the II partition function there will be a measure of averaging-out of those errors, and (ii)the "A-fits" used are expected to be substantially more precise than the raw A-data. Furthermore, such a figure would in any case only be relevant for the most widely-separated II states, since otherwise the standard deviation of the relative canonical free energy will itself be less, falling off roughly as the square root of the corresponding density/temperature separation of the states. The errors are thus, at most, comparable to the thickness of the curves in figure 2.

It is of interest to examine these II chemical potentials as a function of density, rather than pressure, and also to compare them with the estimated chemical potentials within the *canonical* ensemble [1] (which were of course estimated from the *same* TDSMC data). In figure 3 the II results are plotted as a function of the inverse of the mean specific volume (i.e. $1/\langle v^*\rangle^{\mathrm{II}}$, the determination of which is described below), and the canonical as a function of the density $p^* = 1/v^*$. For visual clarity, the results are displayed for only four equally-spaced temperatures (of the 171 temperatures studied). (There is in fact no precise way of putting these canonical and II relative chemical potentials on a common scale, because the equations of state need not exactly coincide anywhere within the range of states studied. In practice the canonical data shown in the figure have been shifted by a common constant to give values roughly similar to the II for states well removed from the coexistence region. One notes that the II data span a range of mean density which is smaller than that of the canonical results, in accord with the discussion of pressure-range limitations in the preceding section. This is raw canonical data, in this case noisier than the II since it involves the estimated pressure, a first-order quantity; μ data from the A-fit would look smooth like the II results).

In this presentation of the II data, one sees at high temperature a smooth increase of chemical potential with density, but for lower temperatures (below criticality) a nearly-horizontal portion corresponding to a very rapid increase of density as the chemical potential increases. This is associated with liquid–gas coexistence; in the thermodynamic limit the isotherms would of course be strictly horizontal within the coexistence density gap. It helps in understanding these chemical potential results, and also those of other thermodynamic properties presented below, if we recall the physical nature of the II states in question. It is easy to plot the density distribution in each (N, p^*, T^*) state (it is just proportional to the terms in the density sum (11) used to evaluate the partition function, cf. equation (1)). Figure 4 shows such distributions for three pressures at a subcritical temperature $T^* = 1.24$. At the lowest pressure shown ($p^* = 0.084$), the system is gaseous, and we see only

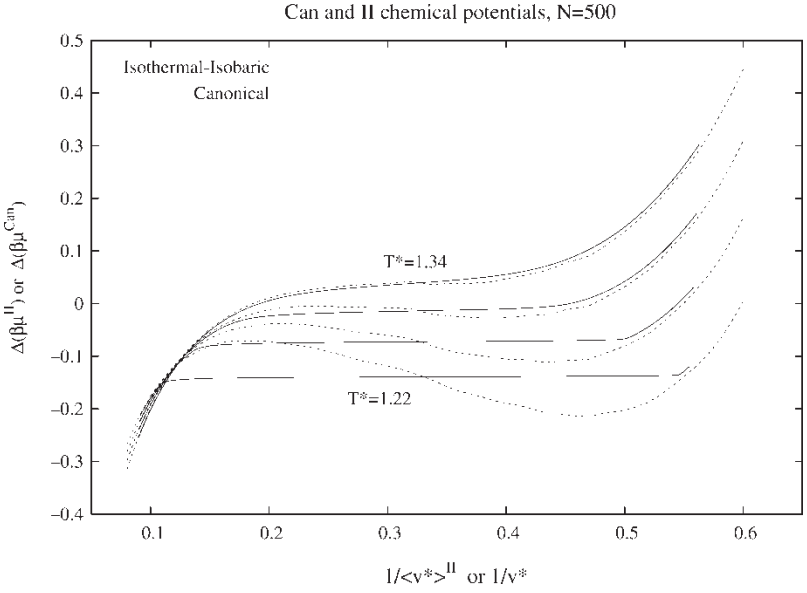

Figure 3. Comparisons of the isothermal–isobaric and canonical chemical potentials along several isotherms.

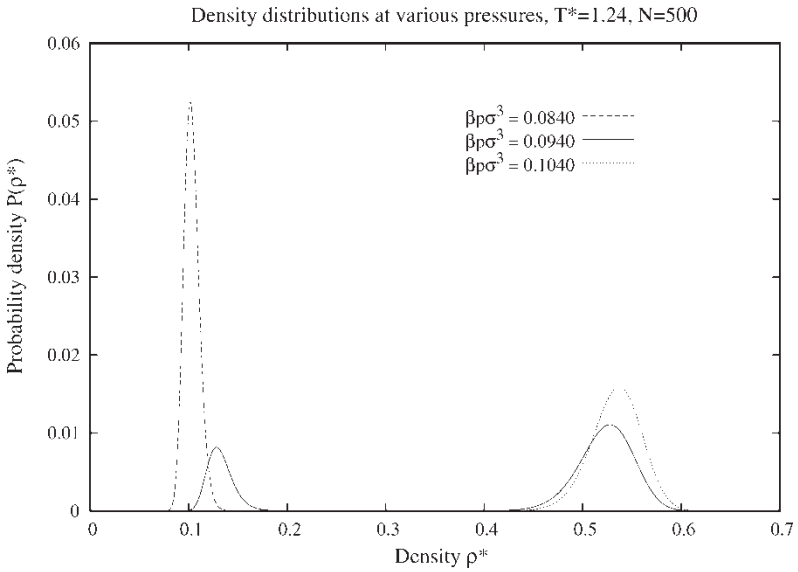

Figure 4. II density distributions for three different pressures, at $T* = 1.24$, $N = 500$. The lowest pressure corresponds to the gas and the highest to the liquid, while the intermediate pressure is such that, in this small system, there is a substantial probability of either phase.

a single peak exhibiting small density fluctuations around the mean; at the highest (0.104) a similar single peak appears around a mean liquid density. This is typical for states like these, well removed from the coexistence region. A small change of pressure in such states leads only to a modest shift of the density at which the peak occurs (of course a shift somewhat larger for the gas than the liquid). For a narrow range of pressures near the vapour pressure we see instead *two* peaks in the density distribution (as here for $p* = 0.094$.), i.e. in the case of small systems, the probability is then divided between the system's being a gas or being a liquid; for the state displayed, the latter turns out to be slightly the more probable. The overall *average* density is a weighted average of those of the two phases. In such a case, a small change of pressure will lead to a *very large* shift of *mean* density, due not primarily to the small shifts in mean density of the two contributing phases, but rather to a very rapid change in their relative probability. This is responsible for the rapid curvature of the chemical potential at pressures near that of coexistence, and for the corresponding near-horizontal portion when it is plotted as a function of density: we are seeing the "rounded" caricatures of the behaviour of macroscopic systems.

By contrast, the *canonical* chemical potential reflects coexistence by exhibiting a "Van der Waals loop". The chemical potential values in the two ensembles are therefore very discrepant in this region. This is natural, because quite different physical situations arise in the two cases. In the canonical case (when considering a small system) at densities within the coexistence region, the system will look like neither gas nor liquid, being restricted to an intermediate density and restrained from separating into the two phases by the associated surface free energy "cost" of doing so.

4. Further thermodynamic functions

4.1 First-order quantities

The derivatives of the relative reduced chemical potential $\Delta(\beta\mu^{\mathrm{II}})$, with respect to pressure and temperature, give at once the mean specific volume and enthalpy. In particular, we have the mean reduced specific volume as

$$\langle v* \rangle^{\mathrm{II}} = T* \left(\frac{\partial \Delta(\beta\mu^{\mathrm{II}})}{\partial p*} \right)_T^*. \tag{12}$$

Alternatively, the same quantity can be generated as a direct average (7), by setting $X = V/N\sigma^3$; this yields the same value. It is more usual to exhibit the density, not the specific volume, and to display the dependence of other thermodynamic quantities on density, rather than on specific volume. A quantity natural to accept as a measure of the expected "density" of the system, corresponding to a state in the II ensemble, might be the reciprocal of this mean specific volume (as in figure 3).

Figure 5 shows (solid curves) the inverse mean specific volume, $1/\langle v* \rangle^{\mathrm{II}}$, as a function of the reduced pressure $p*$ along a selection of equally-spaced isotherms for $N = 500$: this is one way of displaying the "pressure equation of state". One can see at the lower (subcritical) temperatures the very rapid change of density with pressure, occurring near the vapour pressure at each temperature and echoing the sudden change of density to be expected at the vapour pressure for a bulk system; the slopes remain quite steep in the region of the critical density even well above the critical temperature (which is near $T* = 1.31$).

There is a certain ambiguity about this choice of $1/\langle v* \rangle^{\mathrm{II}}$ as a measure of the "density" characteristic of the ensemble, however. One could instead directly average the

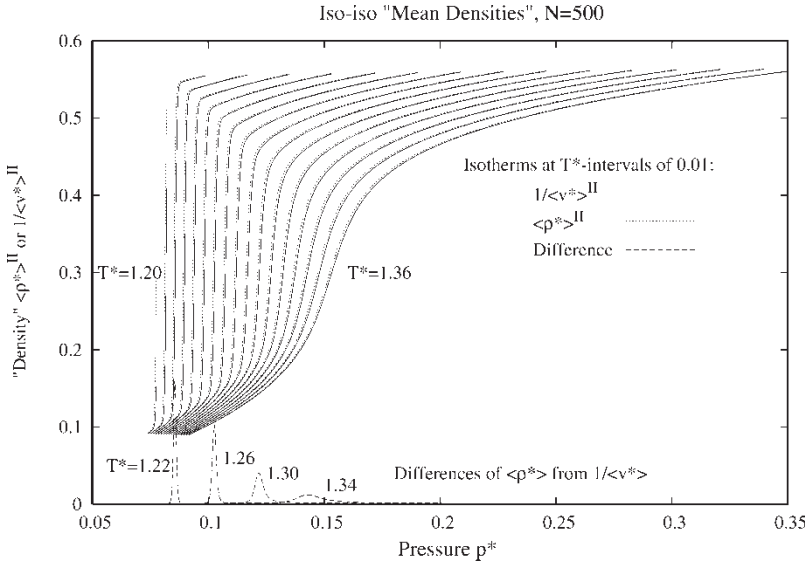

Figure 5. Some isotherms of II "mean density" as a function of pressure. The actual mean density $\langle \rho^* \rangle^{\mathrm{II}}$ and the inverse mean specific volume $1/\langle v^* \rangle^{\mathrm{II}}$ are both shown, along with (dashed) the differences of the two density representations at a few temperatures.

density $\rho^* = N\sigma^3/V$ itself, using equation (7), to obtain as an expectation of "density" the *mean* density $\langle \rho^* \rangle^{\mathrm{II}} \equiv \langle 1/v^* \rangle^{\mathrm{II}}$. Of course *in the thermodynamic limit* (and restricting ourselves to one-phase states) these two proposals for expected density (i.e. $\langle \rho^* \rangle^{\mathrm{II}}$ and $\langle v^* \rangle^{\mathrm{II}}$) will *coincide* (due to the vanishing width of the distributions of density and volume), but this is by no means the case for a small system in the II ensemble (since, in view of the finite relative fluctuations of the volume, we then have $\langle V \rangle \langle 1/V \rangle \neq 1$). The question arises therefore: which quantity to use in describing the II thermodynamics?

The two density-like quantities will of course not coincide for any state of the finite system. We can expect the discrepancy to be especially large near a first-order phase coexistence, since the volume fluctuations may then span the volumes of the two phases; we will see that this is observed. The question cannot easily be ignored, therefore.

In some way, adoption of the mean density $\langle \rho^* \rangle^{\mathrm{II}}$ seems more natural. On the other hand, the mean specific volume v^* seems to play a more fundamental role, being conjugate to the pressure, one of the state-defining variables. As a result, the required ensemble average $\langle v^* \rangle^{\mathrm{II}}$ is given by the pressure derivative of the free energy (as in equation (12) above); no such relation exists for the mean density. It is one of the basic expectations of thermodynamics that knowledge of the dependence of a thermodynamic potential function on the appropriate set of variables defining a state (here μ^{II} in terms of (N, p, T)) should provide a "complete" thermodynamics of the system; if we want this principle to remain part of the (pseudo)thermodynamic description of finite systems, in the II case as in other ensembles, $\langle \rho^* \rangle^{\mathrm{II}}$ does not really form part of such a description, while $1/\langle v^* \rangle^{\mathrm{II}}$ does.

Figure 5 actually shows isotherms of *both* quantities (the $\langle \rho^* \rangle^{\mathrm{II}}$ as dotted curves). These are qualitatively quite similar, showing the expected very rapid rise in the region of coexistence, On the other hand, we see the anticipated large discrepancy between the "density" quantities in that region: these discrepancies are shown explicitly at the bottom of figure 5 for four of the temperatures; they can be quite considerable compared to the value of either. We can readily understand this as due to the fact that the averages include the substantial simultaneous probabilities of two phases of disparate densities. What is more distressing, perhaps, is that rather substantial discrepancies occur even well into the supercritical region. Nevertheless, the distinction between the two "density" measures is not very worrisome in the present context; we will have to return to the question in relation to second-order quantities like compressibility and heat capacity, however (Section 4.2).

In figure 5 we are seeing the pressure–volume equation of state in the II ensemble. It is interesting to compare this with its canonical counterpart, as we do for a few isotherms in figure 6, for the $N = 500$ system. The discrepancy is necessarily very large near coexistence, because the canonical pressure, like the canonical chemical potential, passes through a "Van der Waal's loop". Although the pressure equations of state in the two ensembles agree very well at low, "gas", densities, the II pressure somewhat exceeds the canonical, for these small systems, at higher, "liquid", densities, even well outside the coexistence region. This figure treats $1/\langle v^* \rangle^{\mathrm{II}}$ as the measure of "density" in the II ensemble; however, in view of the small difference between this and $\langle \rho^* \rangle^{\mathrm{II}}$ for states outside the coexistence region, the difference from the canonical is essentially the same for either choice.

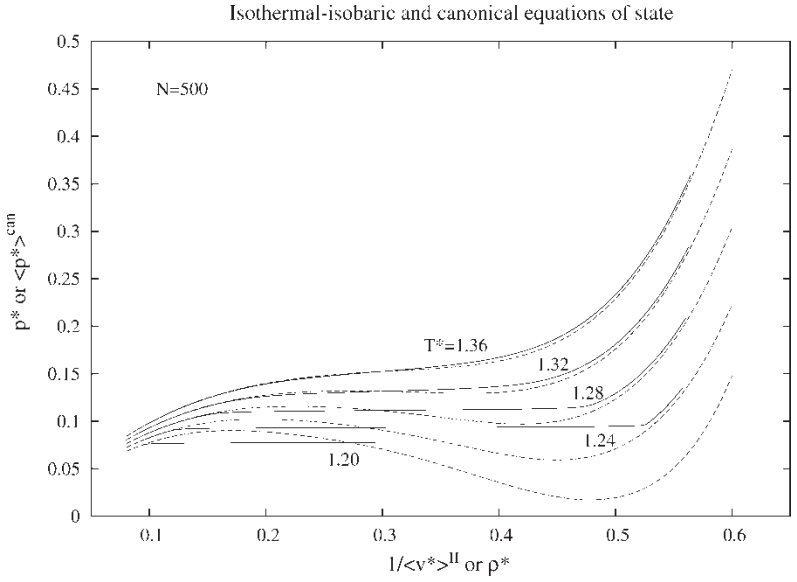

Figure 6. Comparison of the equations of state in the II and Can cases, generated from the same TDSMC data.

($T* = 1.32$ is above the expected bulk critical temperature and also that of a system of this size in the II ensemble (as demonstrated below) and accordingly the corresponding isotherm shows no regions of sharp curvature; this temperature is however below the *canonical* finite-system critical temperature for a system of this size (cf. [1]), and the canonical pressure thus continues to display a small Van der Waal's loop).

Turning to energy-like quantities, the expectation value of the reduced enthalpy is easily obtained as a first derivative of the relative chemical potential:

$$\langle \beta H/N \rangle^{\mathrm{II}} = -T* \left(\frac{\partial \Delta(\beta \mu^{\mathrm{II}})}{\partial T*} \right)_{p*}. \qquad (13)$$

(The interval of $T*$ used in the (five-point) temperature derivatives was 0.001, as mentioned previously). Equivalently, one can obtain $\langle \beta H/N \rangle^{\mathrm{II}}$ as a direct average (as in equation (7)) of $(\langle \beta E/N \rangle^{\mathrm{Can}} + p*v*/T*)$, arriving at the same value. Figure 7 shows a selection of equally-spaced isotherms. One sees at subcritical temperatures the very rapid decrease of enthalpy associated with the rapid progress of the system from gas to liquid as pressure increases near the vapour pressure. (The bulk critical temperature is near $T* = 1.31$, shown dashed). The statistical errors will be comparable to those of the canonical energies [1] (typically around 0.002, at most), but may probably be somewhat smaller due to averaging of errors in carrying out the density sums (see equations (6),(7),(9)) which lead to II results.

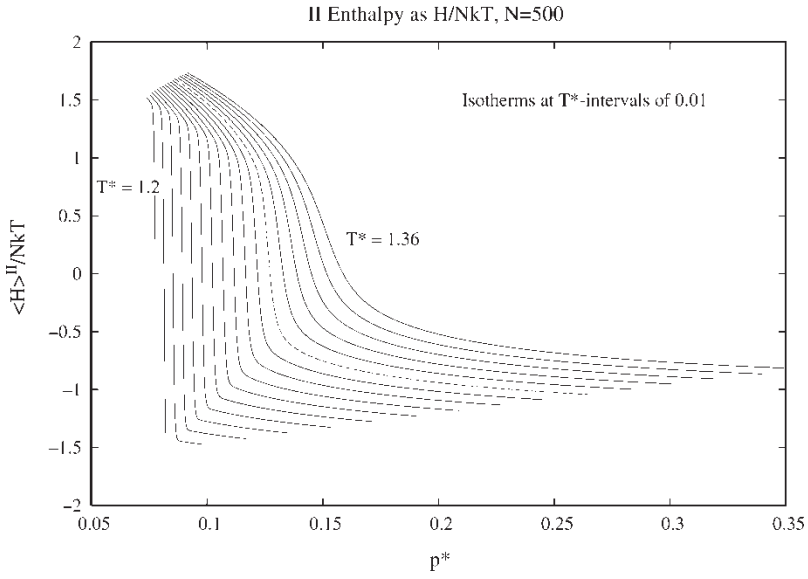

Figure 7. Some isotherms of II specific enthalpy as a function of pressure. (The dashed curve is at a temperature close to critical).

The internal energies are easily obtained from the enthalpies by subtracting from $\langle \beta H/N \rangle^{\mathrm{II}}$ the reduced pV-product, $p^*\langle v^* \rangle^{\mathrm{II}}/T^*$, using the values of $\langle v^* \rangle^{\mathrm{II}}$ already described. Alternatively, one can directly volume-average $\langle \beta E/N \rangle^{\mathrm{Can}}$ (cf. equation (9)); or the mean reduced canonical internal energy comes from adding the reduced kinetic energy per particle (i.e. 1.5) to the canonical average potential energy obtained by differentiating with respect to temperature the algebraic A-fit of the reduced canonical relative Helmholtz excess free energy. The routes to the internal energy are equivalent and give the same estimates. If plotted as a function of pressure, the shapes of the internal energy plots are of course qualitatively similar to those of the enthalpies in figure 7.

It may be of interest to compare these II internal energies in the canonical and II ensembles; this is done at a few temperatures in figure 8. The energies are plotted as a function of the mean density $\langle \rho^* \rangle^{\mathrm{II}}$. At one temperature ($T^* = 1.24$) the plot against inverse mean volume is also shown, for comparison (as a dotted curve): it looks very different in the coexistence region! This difference is entirely that of the two alternative "density" measures used as abscissae, of course. (The mean energy in the coexistence region should be the weighted average over the (relatively narrow) distributions of the densities of the two phases, so one would expect the dependence on *mean density* $\langle \rho^* \rangle^{\mathrm{II}}$ to be essentially linear within the coexistence region; we can see that this is indeed the case. That makes this representation of the data seem the more comfortable here, perhaps). The *canonical* results are shown as dashed lines. At subcritical temperatures the canonical energy is quite different from the II within the coexistence region; this is of course to be expected, since the different ensembles generate quite different physical constitutions for the system in that region. In the canonical case the system's volume and thus density are fixed, and the (small) system is not able to form gas or liquid; by contrast the II states in this region correspond to the system's existing either as gas or as liquid, with a certain relative probability of each. What is actually of more interest is to compare the energies *outside* the coexistence region: there the agreement between the energy results in the two ensembles is remarkably close. This agreement between the ensembles at low and high densities is of course found also at supercritical temperatures. However the discrepancy of the energy isotherms between the two ensembles is clearly found to persist well above the bulk critical temperature in a considerable region around the critical density, as we can see at $T^* = 1.32$ and even at 1.36; this is associated with the rather broad II density distribution in this region. These finite-size effects are of course still larger in the smaller systems that were also studied ($N = 256$ and 72).

4.2 Compressibility and heat capacity

Textbooks usually define the isothermal compressibility according to $\kappa_T \equiv -(1/V)(\partial V/\partial p)_T$, referring to a closed system. It seems natural to estimate the compressibility in a small II system by replacing V in this expression with its mean value. This leads to the following forms for the reduced compressibility $\kappa_T^* \equiv \kappa_T \varepsilon/\sigma^3$:

$$
\begin{aligned}
(\kappa_T^*)^{\mathrm{II}} &= -\frac{1}{\langle v^* \rangle^{\mathrm{II}}} \left(\frac{\partial \langle v^* \rangle^{\mathrm{II}}}{\partial p^*} \right)_{T^*} \\
&= -\frac{1}{\langle v^* \rangle^{\mathrm{II}}} T^* \left(\frac{\partial^2 \Delta \langle \beta \mu^{\mathrm{II}} \rangle}{\partial p^{*2}} \right)_{T^*} \\
&= \frac{N}{T^*} \left[\frac{\langle (v^*)^2 \rangle^{\mathrm{II}} - (\langle v^* \rangle^{\mathrm{II}})^2}{\langle v^* \rangle^{\mathrm{II}}} \right]. \qquad (14)
\end{aligned}
$$

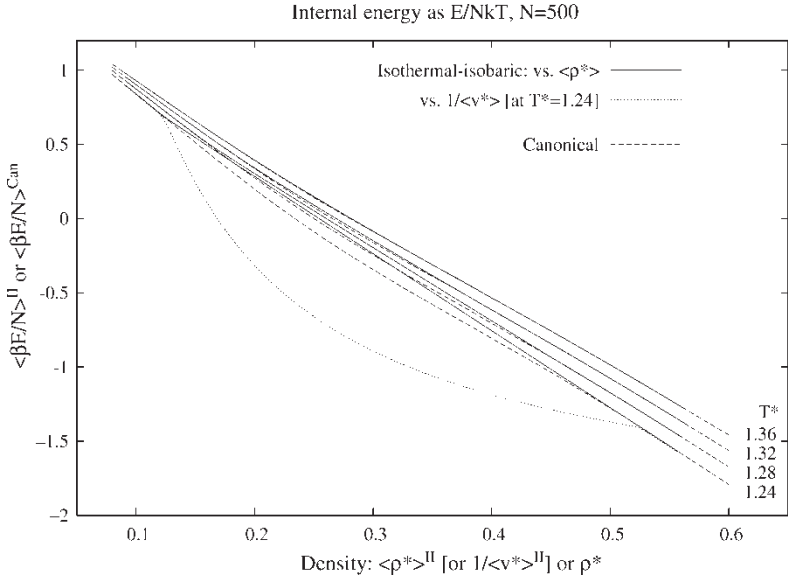

Figure 8. Comparison of internal energy, II and Can, along a few isotherms, for $N = 500$. The II results are plotted against the mean density $\langle \rho^* \rangle^{\mathrm{II}}$; for comparison, the dotted line shows as well the same energy data at $T^* = 1.24$, now plotted against the inverse mean specific volume $1/\langle v^* \rangle^{\mathrm{II}}$.

Thus the compressibility can evidently be evaluated in a variety of alternative ways: by differentiating the previously evaluated mean specific volume, by taking the second derivative of the relative chemical potential, or by calculating the appropriate averages of $(v*)^2$ and $v*$, using (7).

In the thermodynamic limit a *perfectly equivalent* definition of the compressibility is $\kappa_T \equiv (1/\rho)(\partial\rho/\partial\rho)_T$. We discussed in the previous section possible representations of "density" $\rho*$ in the II ensemble. Adopting $1/\langle v*\rangle^{\mathrm{II}}$ leads to the expressions given in equation (14); adopting instead the *mean* density, i.e. $\langle\rho*\rangle^{\mathrm{II}} \equiv \langle 1/v*\rangle^{\mathrm{II}}$, would then give instead the new quantity $(\hat{\kappa}_T^*)^{\mathrm{II}}$:

$$(\hat{\kappa}_T^*)^{\mathrm{II}} = \frac{1}{\langle 1/v*\rangle^{\mathrm{II}}}\left(\frac{\partial\langle 1/v*\rangle^{\mathrm{II}}}{\partial p*}\right)_{T*}, \qquad (15)$$

which can easily be evaluated. Of course for a finite system these two definitions of compressibility no longer lead to identical results. We argued for representing density by the inverse mean specific volume $1/\langle v*\rangle^{\mathrm{II}}$ rather than the mean inverse specific volume $\langle 1/v*\rangle^{\mathrm{II}}$, and thus for equation (14) rather than equation (15), primarily on the grounds that the corresponding thermodynamic description appears more basic, being entirely derivable from the dependence of the thermodynamic potential function μ on its independent variables (N, p, T), as expected in classical thermodynamics. The set of equations (14) emphasizes this pattern of relations; nothing similar exists for $\langle 1/v*\rangle^{\mathrm{II}}$ and $\hat{\kappa}_T^*$.

Figure 9 shows the II compressibility $(\kappa_T^*)^{\mathrm{II}}$ along a few isotherms, both subcritical and supercritical, as a function of pressure (for $N = 500$). At each temperature they peak in the neighbourhood of the vapour pressure; at pressures well below this peak (where the system is gaseous) one sees at each temperature the expected modest compressibility; at pressures above those of the peak the compressibility drops to the much smaller value characteristic of the liquid. (The qualitative behaviour of $(\hat{\kappa}_T^*)^{\mathrm{II}}$ is similar; it has very slightly higher peaks which have their maxima at somewhat lower pressures; of course as the system size increases these peaks become more similar, in the thermodynamic limit coinciding in a delta function). The broad compressibility peaks we see in the coexistence regime are of course entirely an artefact of the small systems studied, in which both phases may appear with finite probability over a substantial pressure range; they reflect primarily the large change in volume associated with changes in the relative amounts of the two phases in response to pressure perturbation, in the pressure range where the phases coexist in a finite II system. The details of the shapes of these *subcritical* peaks are perhaps of only minor physical interest. Of more interest would be the compressibilities of the *coexisting phases* themselves, however, at the (finite-system) vapour pressure, which in principle could play a part in characterising the critical behaviour of the system; these quantities can easily be extracted from the data, and will be considered elsewhere. Compressibilities along some supercritical locus may also be important with a finite-size-scaling analysis in mind, so the observed shapes and magnitudes of the compressibility peaks in that region are of some interest.

Not surprisingly the shapes and heights of the compressibility peaks are noticeably size-dependent. In figures 10 and 11 are shown II compressibilities $(\kappa_T^*)^{\mathrm{II}}$ for two temperatures, one subcritical ($T* = 1.27$) and one supercritical ($T* = 1.35$), for the system sizes studied, $N = 500$, 256 and 72, as a function of $1/\langle V*\rangle^{\mathrm{II}}$. We see the expected decrease of the peak heights as the system size decreases, due to the accompanying enhanced restriction of density fluctuations. For comparison, we also show the canonical-ensemble compressibility (for $N = 500$), based on the same "A-fit" of the *same* TDSMC data.

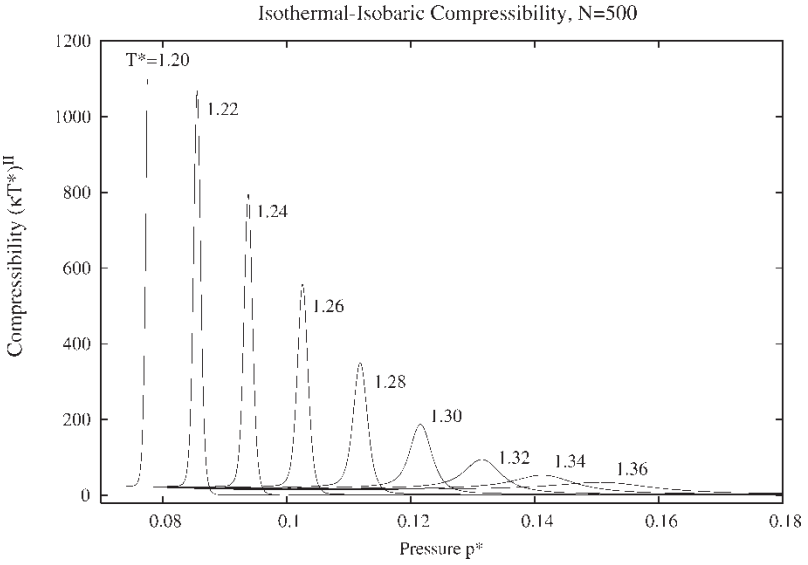

Figure 9. Several isotherms of II isothermal compressibility ($N = 500$). The peaks occur in the region of the vapour pressure (or its supercritical extrapolation); at lower pressures one sees the substantial compressibilities of the gas, at higher the much smaller compressibilities of the liquid.

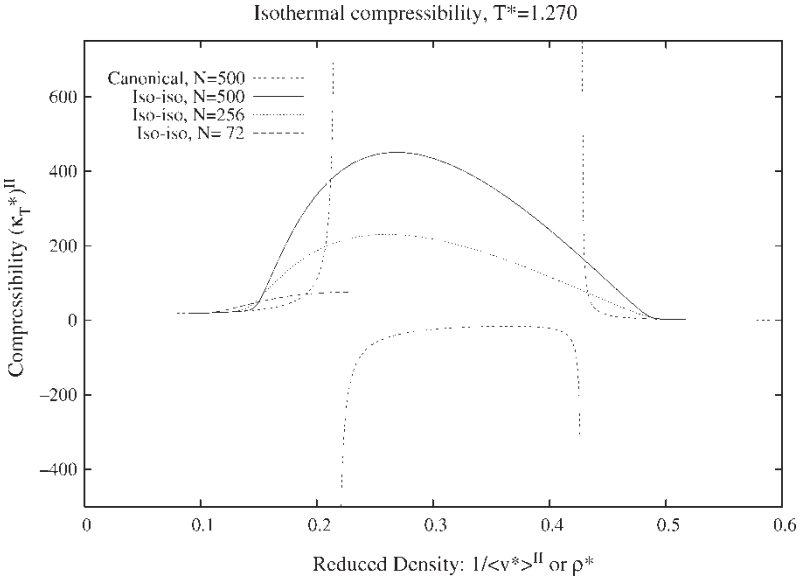

Figure 10. Isothermal compressibility along a subcritical isotherm. II results are shown for different system sizes. For comparison, the canonical behaviour (for $N = 500$) is displayed.

The behaviour at $T* = 1.27$ is characteristic of subcritical temperatures (figure 10), at which the canonical compressibilities must diverge and change sign at densities corresponding to the spinodal points. So in fact within the coexistence region the compressibility behaviours in the two ensembles are necessarily qualitatively different. At densities away from the coexistence region, however, the compressibility results in the two ensembles turn out to agree with each other remarkably well. Above the critical temperature, the behaviour in the two ensembles becomes more similar (figure 11). The canonical peak at $T* = 1.35$ remains much higher than the II, but one must recall that while this is well above the II critical temperature (below $T* = 1.31$), it is only slightly above the finite-system canonical critical temperature (near $T* = 1.33$), where the canonical finite-system compressibility must *actually* diverge (cf. [1]). Again, away from the peak the results in the two ensembles (for the same N) are in excellent agreement.

The isobaric heat capacity $C_p \equiv (\partial H/\partial T)_p$ can be written in several forms relevant to the present model:

$$\begin{aligned}\frac{C_p^{II}}{Nk_B} &= -2T^* \left(\frac{\partial \Delta(\beta\mu^{II})}{\partial T^*}\right)_p - (T^*)^2 \left(\frac{\partial^2 \Delta(\beta\mu^{II})}{(\partial T^*)^2}\right)_p \\ &= T^* \left(\frac{\partial \langle \beta H/N \rangle^{II}}{\partial T^*}\right)_p + \left\langle \frac{\beta H}{N} \right\rangle^{II} \\ &= N\left[\langle (\beta H/N)^2 \rangle^{II} - (\langle \beta H/N \rangle^{II})^2\right]. \end{aligned} \tag{16}$$

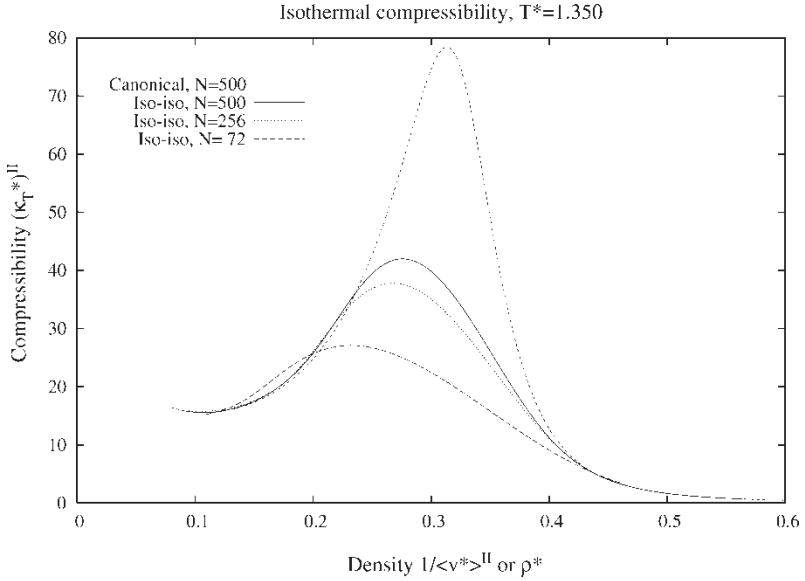

Figure 11. Comparison of compressibilities along a supercritical isotherm.

It can evidently be estimated, equivalently, by taking first and second derivatives of the relative chemical potentials or by differentiating the previously derived specific enthalpies, or indeed by direct evaluation of the enthalpy fluctuations. Figure 12 shows heat capacity isotherms at a selection of temperatures (for $N = 500$). They display broad peaks at pressures near the vapour pressures, broader as the temperature increases, superimposed on the modest background corresponding to the heat capacities of the pure gas or liquid. Once again the finite width of these peaks at subcritical temperatures is of course entirely an artefact of the finite system size: in the thermodynamic limit each subcritical isotherm would have evolved into smooth curves displaying the heat capacity behaviours of the gas and liquid phases, separated, at the vapour pressure, by a delta function (corresponding to the latent heat of vaporization). Finite heat-capacity peaks are nevertheless to be expected in the supercritical isotherms, increasing in magnitude as one approaches criticality.

For some theoretical purposes the "constant-volume" heat capacity is of more interest. A natural definition of constant-volume heat capacity (in a finite system) would be

$$C_v^{\mathrm{II}} = C^{\mathrm{II}}_{\langle v^* \rangle^{\mathrm{II}}} = \left(\frac{\partial E^{\mathrm{II}}}{\partial T}\right)_{\langle v^* \rangle^{\mathrm{II}}}. \tag{17}$$

One convenient way to evaluate this is by differentiation of the energy along loci of fixed mean volume; to do this in the present ensemble, for a particular temperature and specific volume, one first searches, at temperatures adjacent to the one under study, to obtain the pressures giving the desired mean volume, at which pressures the corresponding reduced internal energies are evaluated; these are then numerically differentiated to obtain the corresponding heat capacity. An equivalent alternative is to evaluate the terms of the Yang-Yang expression [10] for C_v, which can be written (with $\mu^* \equiv \mu/\varepsilon$) and adapting it to the finite system by replacing v^* of the thermodynamic expression by $\langle v^* \rangle^{\mathrm{II}}$) as

$$\frac{C_v^{\mathrm{II}}}{Nk_B} = \langle v^* \rangle^{\mathrm{II}} T^* \left(\frac{\partial^2 p^*}{\partial T^{*2}}\right)_{\langle v^* \rangle^{\mathrm{II}}} - T^* \left(\frac{\partial^2 (\mu^*)^{\mathrm{II}}}{\partial T^{*2}}\right)_{\langle v^* \rangle^{\mathrm{II}}}; \tag{18}$$

one need only find the required second temperature derivatives of the pressure and chemical potential along loci of fixed $\langle v^* \rangle^{\mathrm{II}}$. (The derivative of the reduced chemical potential is easily written in terms of the first and second derivatives of $(\beta\mu)^{\mathrm{II}}$.)

Figure 13 shows results, for various N, as a function of the inverse mean volume, along a typical sub-critical isotherm ($T^* = 1.26$). The highly skewed shape of these curves within the coexistence region is of some interest. In fact in the *thermodynamic limit* and within the coexistence region $p^* = p^*_{\mathrm{vap}}(T^*)$ and $\mu^* = \mu^*_{\mathrm{coex}}(T^*)$, so the derivatives in equation (18) become independent of density; it follows that the heat capacity *Cv/NkB* should be linear in the specific volume within this region, thus continually decreasing as the mean density increases. The present II results show a much-rounded approximation to that behaviour. (For illustrative comparison, the dotted curve labelled "limiting shape" indicates the result of using, in the Yang-Yang formulation, our measured $N = 500$ vapour pressures and coexistence chemical potentials (the determination of which is described in the following section), and for the specific volume its mean value $\langle v^* \rangle^{\mathrm{II}}$. This curve thus approximates the limiting *shape* (though not necessarily the limiting magnitude); we can see that our finite-system isotherms are slowly approaching this shape as the size increases).

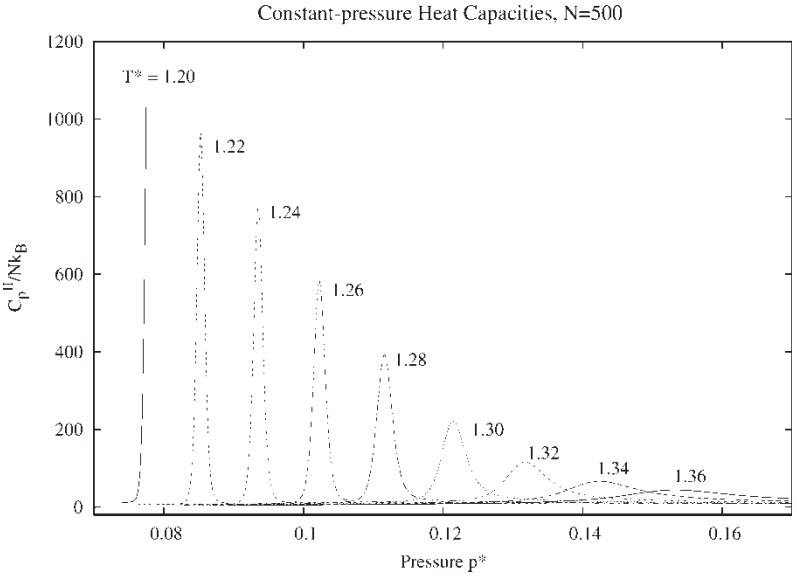

Figure 12. Several isotherms of the constant-pressure heat capacity C_p^{II}. Once again there are peaks in the coexistence region (which would turn to delta-functions representing the latent heats, in the thermodynamic limit). The peaks are superimposed on the background heat capacity of the gas and liquid phases.

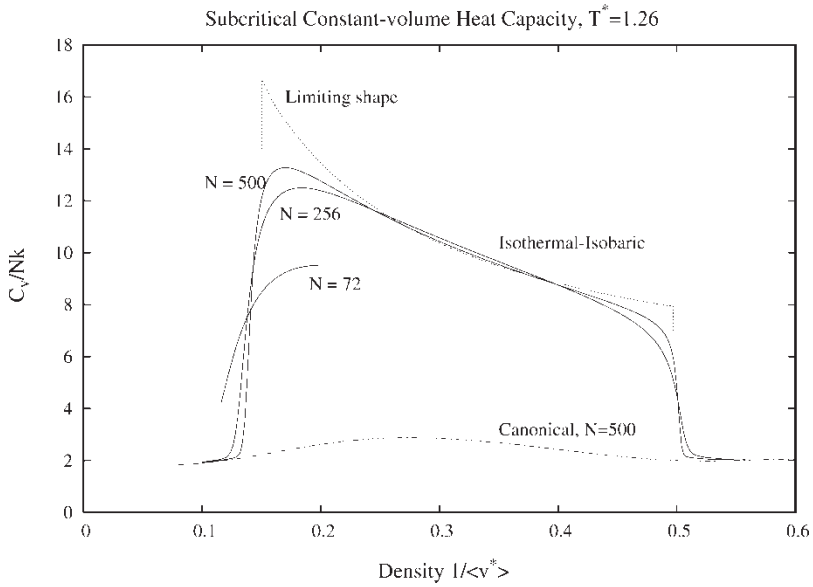

Figure 13. Constant-volume II heat capacities along a subcritical isotherm. The skewed nature of the isothermal–isobaric results within the coexistence region is noticeable; it is discussed in the text, along with the meaning of the dotted curve labelled "limiting shape". The very different behaviour of the canonical heat capacity is also shown (dot-dashed).

Figure 13 also shows the *canonical* heat capacity: this shows only a relatively weak peak in the coexistence region. This is not surprising: only minor density fluctuations are possible in the small canonical system, while in the II they may be large—in particular, they are dominated by fluctuations in the proportions of the two phases, of widely-different energies. Looking at it in another way, only small changes of structure accompany a small temperature change in the canonical case, while it introduces a shift in the proportions of the phases under II conditions.

The following figure 14 displays (solid curves) the constant-volume heat capacity along several supercritical isotherms (with $N = 500$). We see the expected peaks near the critical density, echoes of the divergence of the heat capacity at criticality in the thermodynamic limit, and the expected increase in their height as one approaches the critical temperature. (For smaller systems the peak heights are modestly smaller, but essentially similar). For comparison the figure also shows the *canonical* isochoric heat capacity at one of these temperatures, namely $T* = 1.34$. This shows a very much more modest

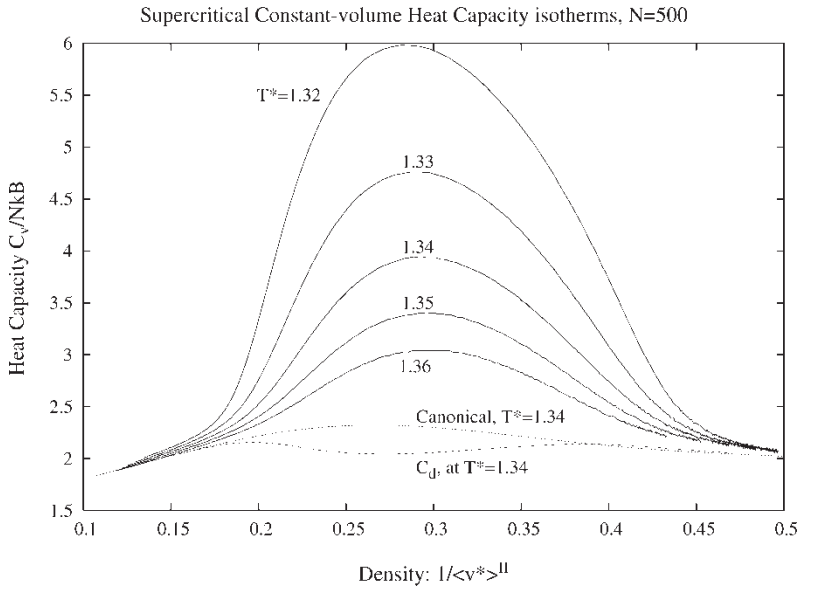

Figure 14. Some supercritical isotherms of II constant-volume heat capacity ($N = 500$). The figure also shows, for $T* = 1.34$, the canonical result (dotted) and the at-first-sight surprising behaviour of the constant-density heat capacity (dashed).

maximum, as expected since the density fluctuations associated with criticality are of course severely constrained in a small canonical system. In short, the physical state corresponding to a small system of fixed overall density is totally unlike that in which the overall density may fluctuate, so the substantial difference of behaviour of heat capacities in the two ensembles in that region is in no way surprising. The canonical heat capacity turns out to agree rather well with the II at densities well below the peaks, however.

We discussed above the ambiguity regarding the definition of "density" in finite-size II systems; this question arises again with respect to the "isochoric" heat capacity. Macroscopically, this heat capacity is defined with closed systems in mind, so that the "constant-volume" heat capacity can as well be considered a "constant-density" heat capacity, which we might write

$$C_d^{\mathrm{II}} \equiv C^{\mathrm{II}}_{\langle 1/v^* \rangle^{\mathrm{II}}} = \left(\frac{\partial E^{\mathrm{II}}}{\partial T} \right)_{\langle 1/v^* \rangle^{\mathrm{II}}} \tag{19}$$

Once again, this quantity will coincide with C_v^{II} (equation (17)) in the thermodynamic limit, but will differ in value for a finite II system. The differences can even be a bit surprising: for the present systems the corresponding C_d isotherms actually show *minima* near the critical density! (By way of example the $T^* = 1.34$ C_d - isotherm is shown (dotted) in the figure). Minima are also displayed by C_d within the coexistence region at subcritical temperatures for these small systems. Evidently the definitions C_v^{II} and C_d^{II} lead to *qualitatively* different behaviours for small systems under certain conditions; for these small systems the former evidently has behaviour more consonant with our macroscopic expectations and so is more useful.

Figure 15 displays the *temperature* dependence of C_v/Nk along isochores for several values of $1/\langle v^* \rangle$. At low temperatures we note that the heat capacity depends monotonically on density, as implied by the above discussion of the skewed shapes of figure 13, while at high temperature it is instead for densities near the critical density that the heat capacity takes the highest values. (Among the densities shown, 0.30 is very close to the critical density). One sees for such densities the expected rise of the heat capacity as the temperature is decreased toward critical, and a weak maximum somewhat below the critical temperature as the temperature is further decreased: the rounded and shifted peak to be expected in a finite system.

5. Gas–liquid coexistence

We use the TDSMC data to explore the II gas–liquid coexistence properties. Specifically, we would like to know the coexisting densities, the vapour pressure and the relative chemical potential at equilibrium, along with the remaining thermodynamics of the transition, as a function of subcritical temperature. We have already noted that it is easy to generate the density distribution at any temperature and pressure (cf. figure 4), and that for a range of pressures and at sufficiently low temperatures this distribution consists of two well-separated peaks. Coexistence equilibrium corresponds to equal probabilities for the two phases, i.e. to equal areas for the two peaks. (The thermodynamic argument for this notes that such an area is proportional to the partition function Γ for the phase (cf. equation (1)) and thus our condition corresponds to equal chemical potentials for the coexisting phases). As long as the probability becomes extremely small for some densities between the peaks corresponding to the two phases (so they are well-separated) this provides an unambiguous identification of the coexistence conditions.

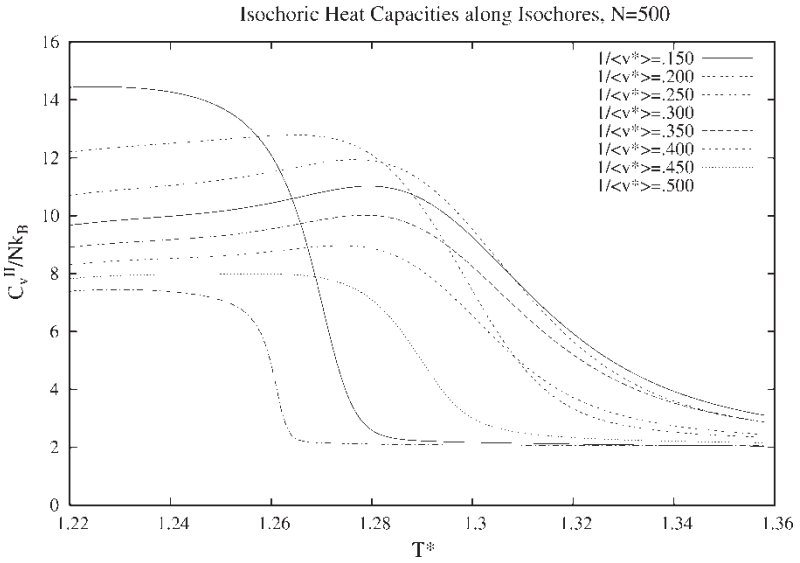

Figure 15. Temperature dependences of the constant-volume II heat capacities along several isochores.

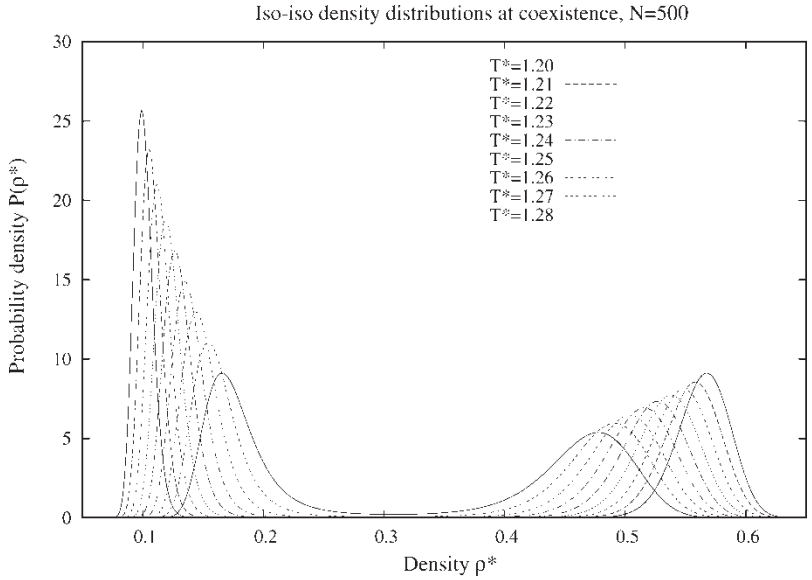

Figure 16. Isothermal–isobaric density distributions at equilibrium (i.e. at the vapour pressure) at several subcritical temperatures.

Of course in finite systems, at temperatures not far below critical, the peaks "overlap" (i.e. are not distinct) and it becomes impossible to apply this criterion. (It is likewise impossible to use conventional single-state II (or grand canonical) simulations to find the properties of the phases reliably in this near-critical temperature regime, of course).

For each temperature (at intervals of 0.001 in T^*) the pressure was adjusted to satisfy this coexistence criterion. Figure 16 shows the resulting coexistence density distributions for a few temperatures (with $N = 500$). The corresponding pressures are the II reduced vapour pressures, shown in figure 17 along with some for $N = 256$ (solid and dashed curves respectively). (For $N = 256$ the accessible temperature range was restricted (at low temperatures) by an inadequate TDSMC density range, as mentioned previously, and (at high temperatures) by the requirement for well-separated density peaks; for $N = 72$ these difficulties left *no* accessible temperatures. The former problem could easily have been solved by examining a slightly broader density range in the original TDSMC run; the latter is however inherent, though less severe as the system size increases). The $\diamond$ symbols indicate the corresponding II critical points for the two temperatures, estimated by a "mixed-field finite-size scaling" procedure described below; they form very plausible extrapolations of the vapour

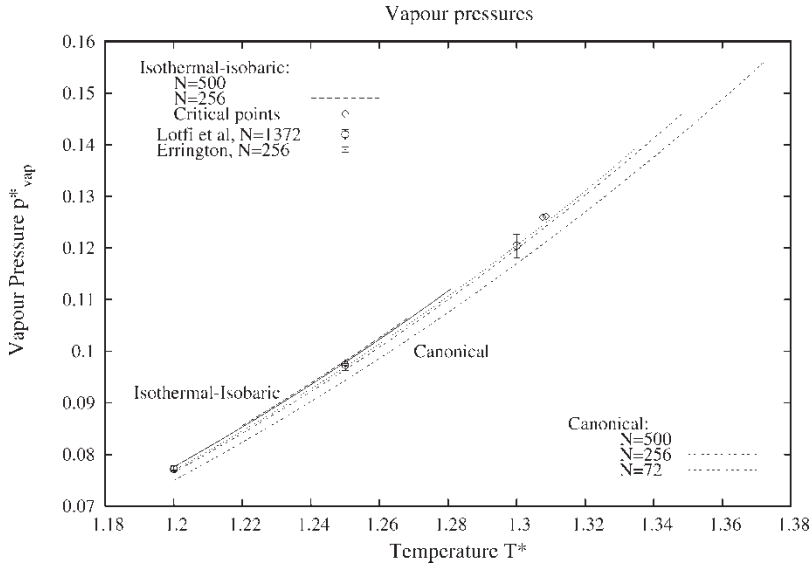

Figure 17. Estimated II vapour pressures (solid and simple dashed curves) at $N = 500$ and 256. The figure also shows the corresponding *canonical* vapour pressures (with a much larger temperature dependence, in the opposite sense). The $\diamond$ symbols indicate the critical points estimated below. Previous II estimates are also indicated, by points with errorbars.

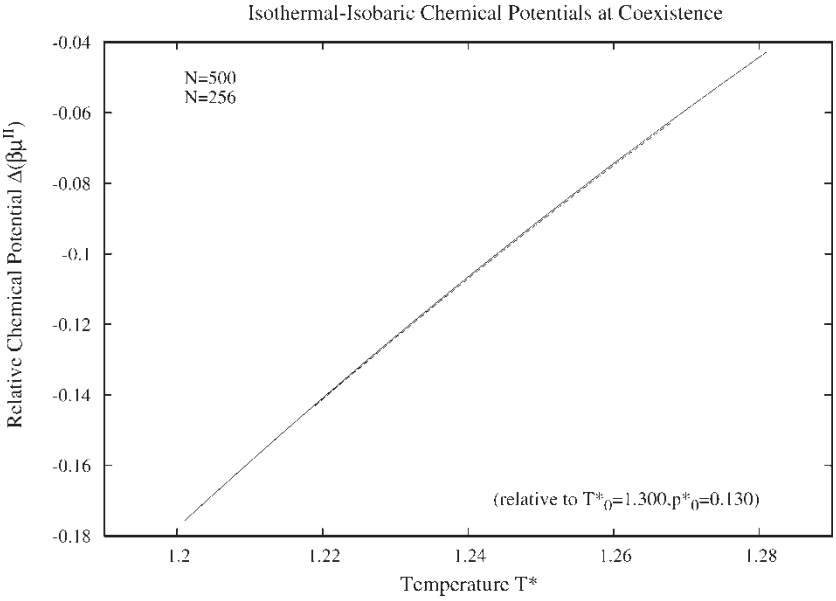

Figure 18. II chemical potentials at coexistence.

pressure curves. The statistical error in the II vapour pressures can be estimated by finding what shift of pressure would lead the logarithm of the ratio of the areas under the two peaks to equal the likely uncertainty in the relative values of $\beta N\mu^{\mathrm{II}}$ for the phases (cf. equation (3)); to equate this to the uncertainty of relative values of βA^{Can} for the corresponding density gap should overestimate the error, since it ignores both the smoothing of the fit, "A-fit", made to A^{Can} and the averaging that occurs in estimating $\beta\mu^{\mathrm{II}}$ (cf. equation (2)). This (over)estimate of the error in the II vapour pressure varies from 0.11 to 0.15% as the temperature goes from 1.20 to 1.28: i.e. $\sim$0.0001, too small to appear on figure 17.

There exist only very few other high-quality Monte Carlo estimates of the II vapour pressure for the present version of the Lennard-Jones model (cf. table 4 of [1]). Figure 17 shows the estimates at $T* = 1.20$, 1.25 and 1.30 for $N = 1372$ due to Lotfi *et al.* [11], and at the lower two temperatures for $N = 256$ by Errington [12]. (The former appear to be consistent with ours within their (relatively large) estimated uncertainty. If our error estimate and that of Errington (quite small) are both sound, these two sets of results are marginally discrepant).

Figure 17 shows as well very precise *canonical* vapour pressures obtained from (the same) TDSMC data [1]. (It is noteworthy that these latter are available over a wider range of temperatures: no problem of overlapping density distributions arises when applying the "double-tangent" construction, so one can derive co-existence data right up to the canonical finite-system critical region, itself at a temperature high relative to the bulk system). The II vapour pressures *decrease* with system size, while the canonical *increase*; the bulk vapour pressures presumably lie between them, and thus are evidently very closely constrained by these two sets of results. Figure 18 shows chemical potentials at coexistence (all relative to the arbitrary reference state specified above); the estimated errors are $\sim$0.0005. The coexistence chemical potentials display very small size-dependence.

The properties of the separate coexisting phases may easily be found by averaging over only the volumes relevant to that phase (at the vapour pressure, and of course at temperatures where the density distributions corresponding to the phases are clearly separated). In particular we can easily find the mean specific volume or density of each coexisting phase. In figure 19 we show the corresponding mean densities $\langle\rho*\rangle^{\mathrm{II}}$ of each phase as a function of temperature for $N = 256$ and 500: i.e. the "coexistence curves"; also shown is the average of the mean densities of the coexisting phases: i.e. the "rectilinear diameter". The Figure also shows the corresponding canonical coexistence curves (generated from the same TDSMC data). The II curves show a smaller density gap between the phases, and one which, as expected, narrows more quickly as temperature is increased (corresponding to the lower effective critical temperatures consistent with less constrained fluctuations). The N-dependence of the II curves is as expected much smaller than that of the canonical, and it is in the opposite sense, so that the curves in the two ensembles are almost surely bracketing those of the thermodynamic limit. (If the coexistence is portrayed by plotting the inverse mean specific volumes $1/\langle v*\rangle^{\mathrm{II}}$ instead of mean densities, it leads to a small shift of (all three) curves to lower values; the shift ranges from $\sim$0.0008 at the low temperatures up to $\sim$0.0045 near $T* = 1.28$.)

Results from the investigations of Lotfi *et al.* [11] and Errington [12] are also shown. (At $T* = 1.30$ the gas density estimated in the former work is clearly

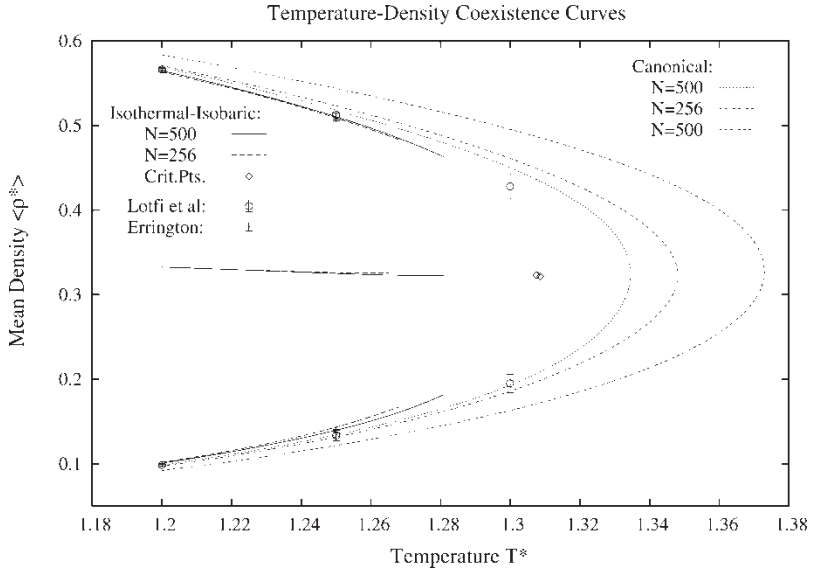

Figure 19. Coexistence data. The symbols match those of Figure 18.

too small (especially in view of their estimate of $T_c^* = 1.31$); there is of course special difficulty about getting precise II data so close to criticality. This discrepancy was already made clear by comparison with some results for a closely similar model, due to Shell *et al.* [13]).

It is similarly easy to calculate other thermodynamic properties of each of the coexisting phases and thus to investigate the thermodynamics of the liquid-to-gas transition—the latent heat and so on. In figure 20 are shown $\Delta\langle v*\rangle$, $\beta\Delta\langle H\rangle/N = \Delta S/Nk_B$, $\beta\Delta\langle E\rangle/N$ and also $\beta\Delta A/N = -p*\Delta\langle v*\rangle/T*$ as a function of temperature, for $N = 500$. They differ from the canonical results (dotted curves) in conformity with the facts that the density gap between their coexisting phases is smaller, and that it also decreases more rapidly as the temperature rises. (The ΔS estimate of [11] (actually for $N = 1372$) is again implausible at $T* = 1.30$.)

It is also feasible to calculate the compressibilities and heat capacities of each of the coexisting phases separately. These can be obtained for example by finding the volume and energy fluctuations of the phases, or alternatively by calculating the consequences for each phase separately of small perturbations of pressure (around the vapour pressure) or of temperature. The temperature dependences of subcritical compressibilities and heat capacities of the two phases at coexistence are of particular interest in examining the approach to criticality. We defer

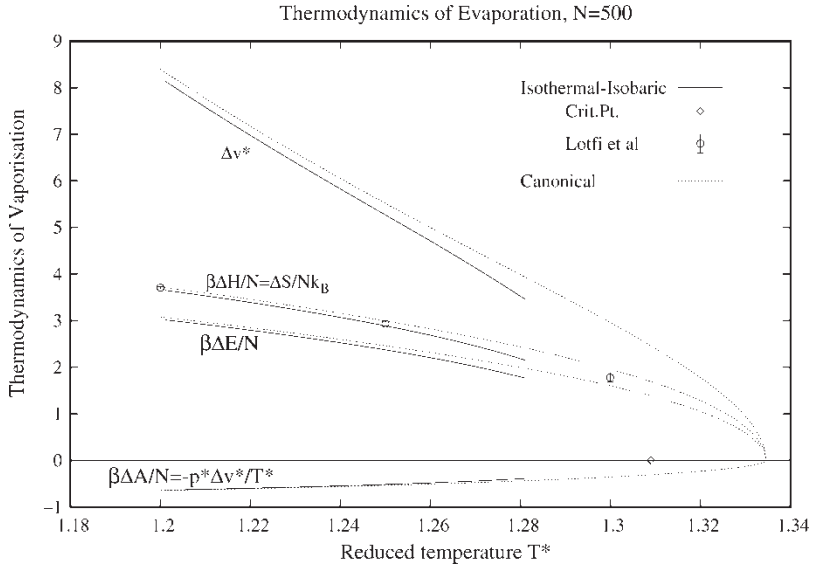

Figure 20. Further thermodynamic characteristics of the liquid–gas transition, as estimated from the same TDSMC data, for both the isothermal–isobaric and canonical ensembles.

presentation of such data to another publication with that particular focus; here we take only a cursory look at examining critical behaviour.

It is easy, for example, to examine the "order parameter", which we may take to be the "density" gap between the phases, $\Delta\left(1/\langle v^*\rangle\right) \equiv 1/\langle v^*\rangle_{\text{liq}} - (1/\langle v^*\rangle_{\text{gas}}$. Since the Lennard-Jones fluid is believed to be "Ising-like", we may expect this to narrow, with temperature increase, as $(T_c - T)^\beta$, plus correction terms, with $\beta \approx 0.326$. (This exponent β should not be confused with $\beta = 1/k_B T$.) As a naive approach to analysis of the data it is therefore natural to plot the order parameter to the power $1/\beta$ against the temperature: if we were able to neglect the correction terms, we would expect this to be linear with an intercept of T_c for large systems. Small systems, however, would be expected to revert ("cross over") to "mean-field" behaviour near to the critical temperature, due to their inability to contain the full "thermodynamic" density fluctuations. Such plots are shown in figure 21 for $N = 256$ and 500 (dashed and solid curves). Over the accessible temperature range there is no very clear finite-size crossover. The curves are very slightly convex, but considerably closer to straight than the corresponding canonical order-parameter curves (based on the same Monte Carlo data and also shown). They may merit further analysis, although without very large correction terms their intercepts must occur at temperatures well below the estimated critical temperatures.

Wilding and Bruce [14,15] proposed that an appropriate linear combination of the particle and energy densities—the "mixed operator" M—should, at criticality, have a distribution matching that of the order parameter (the "magnetisation") of the Ising model at its critical point. One can examine this by searching for an appropriate "mixing coefficient" of the linear combination which, in conjunction with proper choices of a pressure and a temperature, lead to the expected distribution: the required pressure and temperature should then be those of the critical point (of the finite system). This analysis has been applied to several model systems with apparent success; the extension to II distributions (using N rather than the volume as the "size" parameter) was proposed by Wilding and Binder [16], and applied with apparent success to a truncated Lennard-Jones system. Fisher *et al.* [17,18] have since pointed out that such "mixed-field finite-size scaling" may not be fully accurate in case the so-called "Yang-yang anomaly" exists (i.e. that the chemical potential derivative term, in the Yang-Yang expression (18) diverges along with the pressure term, at criticality), so that a more searching analysis may in fact be necessary in order to find precise critical behaviour; the present data may be appropriate for such an analysis.

It nevertheless seems interesting in the meanwhile to examine the present data in the Wilding-Bruce manner. The required critical Ising distribution was generated from the highly accurate determinations of Tsypin and Blote [19]. At a given temperature the pressure was adjusted to ensure equal contributions to the second moment of the distribution of the "mixed operator" from values above and below its mean, while the "mixing coefficient" was meanwhile chosen to ensure equal heights for the two maxima in its near-critical distribution; the resulting critical temperatures estimates were then those that gave most nearly the expected critical ratio of the maxima to the minimum of the distribution adjusted in this way. During this optimization the required distribution was completely recalculated from the A-fit to the original TDSMC data, for each trial set of the three parameters. In figure 22 results can be seen for $N = 500$ (open circles) and $N = 256$ (open squares), along with the corresponding Ising distribution at criticality (solid curve). (For the sake of clarity, only a small selection of the many—six hundred—II data points calculated along each distribution have been displayed; in contrast to

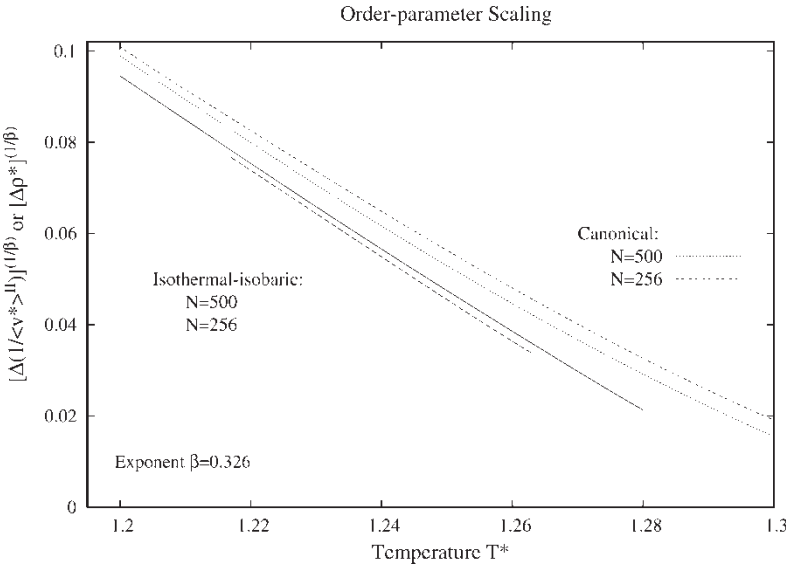

Figure 21. Naive order-parameter scaling plots, for both ensembles, assuming that Ising-like behaviour is expected.

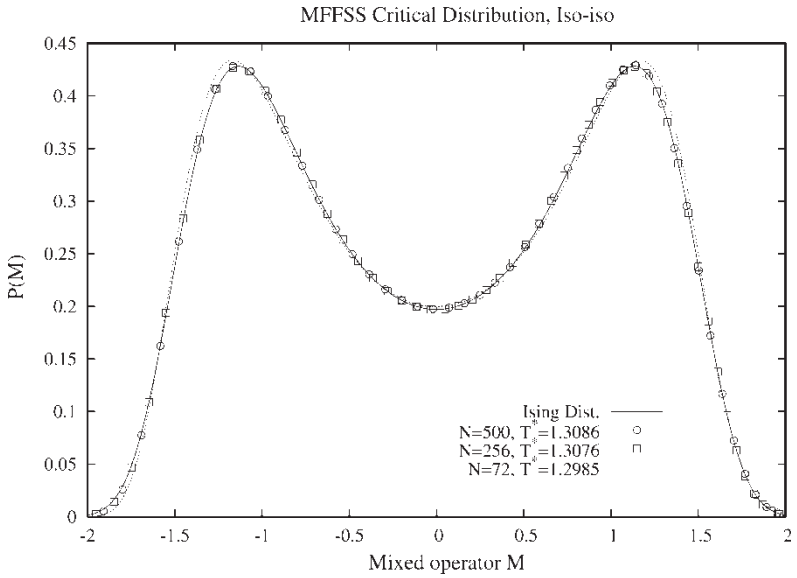

Figure 22. Mixed-field finite-size-scaling plots (cf. [13]) from the isothermal–isobaric data, for the various system sizes, (The results for the small system, $N = 72$, cannot be made to match the Ising reference distribution).

conventional II results, we are of course able to generate our distributions on an arbitrarily fine grid). The resulting matches of the distribution are strikingly good. Critical points estimated in this way were shown in figure 17; one can see that they belong to entirely plausible extrapolations of the corresponding vapour pressure curves. The goodness of the fit is very sensitive to the temperature, so that there is in this sense no difficulty in choosing the "best" temperature to the *precision* quoted (of about 0.0001). It does not however follow that one has determined the relevant temperature so *accurately*. In fact if a similar analysis is carried out using the TDSMC (3S) data set obtained using segmented sampling (see ref. [1]), i.e. a completely independent data set of similar high precision, the resulting "critical" temperatures may disagree by amounts of the order of 0.001; one must suppose errors of that order in each such determination, therefore, and also in any eventual extrapolation towards the bulk critical temperature. (It is also the case that matching to an alternative good determination of the universal critical Ising distribution [20], using the present fitting criteria, by itself leads to shifts ~ 0.0005 in the "best' temperature. The precise fitting criteria used can also have an effect, and they have not always been made clear in published applications.)

The similar best-fit results for the smallest system ($N = 72$) also appear in figure 22, shown as a dotted line. It is evident that in this case the match is however quite inadequate. (This was also the case for the small system when using the segmented (3S) TDSMC data [1]: we expect it to be characteristic of such small systems. It is true that the density range of the $N = 72$ TDSMC results was not quite great enough to generate the whole of the high-M tail of the distribution of the "mixed operator" M. In carrying out the required second-moment symmetrization the M-range was therefore truncated symmetrically; we find that similar truncation does not materially alter the analysis if applied to the larger systems, however, and do not believe this is connected to the poor match).

The finite-system critical temperatures obtained in this way are expected [14] to approach the bulk value as $1/N^{(1+\theta)/3\nu}$, where θ and ν are exponents describing the approach to criticality of Ising-like systems (correction-to-scaling and correlation-length exponents respectively). In view of the inadequacy of the $N = 72$ result we have useful estimates only for two sizes, $N = 500$ and $N = 256$, so we are unable with the present data to *test* conformity to this relation. Assuming it to hold, we can use our results to estimate the bulk critical temperature; this leads to the value $T_c^* = 1.309$ (with, as mentioned, a probable error of at least ~ 0.001).

More detailed analysis of the critical behaviour is postponed to a later publication.

6. Conclusion

It seems natural to generate the thermodynamics of a model system in the *canonical* ensemble using TDSMC data, as explored in the preceding paper [1]. In this paper we have shown however that the thermodynamics in the II ensemble can similarly be generated from such TDSMC data. This constitutes an alternative method of estimating such II data. For both ensembles considerable ranges of the corresponding independent thermodynamic variables can be studied using very few TDSMC runs; for example all of the results reported in this and the preceding paper stem from a single such run.

The precisions of the results for each thermodynamic property or equation of state are comparable in the two ensembles. We believe the results, in both ensembles, to be substantially more precise than those that have been reported on the basis of more conventional simulation

techniques, or than could easily be so generated. Furthermore all the properties are in principle known *continuously* throughout the ranges studied, not merely at isolated states.

Isothermal–isobaric thermodynamic data for model systems has previously been estimated by Monte Carlo simulation in the space ($\mathbf{q}^N$, V), therefore involving steps in which the volume V is allowed to increase or decrease, as well as those simply altering the configuration $\mathbf{q}^N$ by moving one or a few particles. However, the probability of acceptance of a trial move involving any substantial volume change, in a dense fluid, is extremely small (not to mention other complications about such moves). As a result such simulations are ordinarily very inefficient, and the estimates have tended to be imprecise and/or expensive. This paper reports instead the generation of precise II estimates using data generated by a TDSMC run, which (like conventional canonical Monte Carlo runs) requires only single-particle moves: no volume-change steps are involved. This makes it an attractive alternative method. Of course it is true that to estimate the results for a particular single pressure one will need to target a range of densities in the TDSMC run. However one is usually interested in II results for more than one pressure; in that case it will be highly efficient to generate them from TDSMC data (or indeed, for a single temperature, many results could be obtained even from simple "density-scaling" Monte Carlo, DSMC). At the same time, particular convergence problems, such as "critical slowing down", may be avoided.

It is of some interest to have generated the thermodynamics in the two ensembles—II and canonical—from a single set of basic Monte Carlo data, since of course the properties and equations of state depend on the ensemble for the finite systems required in simulation studies: this dependence can be studied in some detail. Such dependences are particularly significant in connection with first-order phase separations such as occur in the Lennard-Jones fluid examined in these papers. (In particular, we have shown the strong dependence of the estimated properties on the ensemble (and the size of the system) at supercritical temperatures but in the vicinity of the critical density).

To carry out analysis of the critical behaviour using modern finite-size scaling methods [17,18] will require estimation of additional properties not reported here. The potential for generating precise and continuous estimates of such data makes the present approach particularly suitable for this purpose, to be addressed subsequently.

Elsewhere [21] the TDSMC data has instead been used to generate the equilibrium behaviour of finite systems in the so-called Gibbs Ensemble. That application of the TDSMC data required the help of an approximation in the form of an interpolation of the TDSMC data to various system sizes N. The results made possible the examination of various perhaps surprising features of the finite-system Gibbs Ensemble, and pointed to some cautions about what properties may in fact be reliably obtained by simulations in such an ensemble. By making a similar approximation, rather precise results in the *grand-canonical* ensemble may be generated, again using the same TDSMC data; this development will be presented in a forthcoming paper.

Acknowledgements

The financial support of the Natural Sciences and Engineering Research Council of Canada is much appreciated. I have had, as so often, useful discussions with Glenn Torrie, Stu Whittington and other associates. Jeffrey Errington kindly supplied some details about his results.

References

[1] J.P. Valleau. Temperature-and-density-scaling Monte Carlo: methodology and the canonical thermodynamics of Lennard-Jonesium. *Mol. Simul.*, (2004) (preceding paper—insert citation).
[2] T.L. Hill. *Statistical Mechanics*. p. 63, McGraw-Hill, New York (1956).
[3] P. Attard. *Thermodynamics and Statistical Mechanics*, Academic Press, London (2002).
[4] R.A. Sack. Pressure-dependent partition functions. *Mol. Phys.*, **2**, 8 (1959).
[5] P. Attard. On the density of volume states in the isobaric ensemble. *J. Chem. Phys.*, **103**, 9884 (1995).
[6] G.J.M. Koper, H. Reiss. Length scale for the constant pressure ensemble: application to small systems and relation to Einstein fluctuation theory. *J. Phys. Chem.*, **100**, 422 (1996).
[7] D.S. Corti, G. Soto-Campos. Deriving the isothermal–isobaric ensemble: the requirement of a 'shell' molecule and simulations of small systems. *J. Chem. Phys.*, **108**, 7959 (1998).
[8] D.S. Corti. Monte Carlo simulations in the isothermal–isobaric ensemble: the requirement of a 'shell' molecule and simulations of small systems. *Mol. Phys.*, **100**, 1887 (2001).
[9] See e.g. L. Fox, D.F. Mayers. *Computing Methods for Scientists and Engineers*, ch. 8, Clarendon Press, Oxford (1968).
[10] C.N. Yang, C.P. Yang. Critical point in liquid–gas transitions. *Phys. Rev. Lett.*, **13**, 303 (1964).
[11] A. Lotfi, J. Vrabec, J. Fischer. Vapour liquid equilibria of the Lennard-Jones fluid from the NpT plus test particle method. *Mol. Phys.*, **76**, 1319 (1992).
[12] J.R. Errington. Direct calculation of liquid–vapour phase equilibria from transition matrix Monte Carlo simulation. *J. Chem. Phys.*, **118**, 9915 (2003).
[13] M.S. Shell, P.G. Debenedetti, A.Z. Panagiotopoulos. Generalization of the Wang-Landau method for off-lattice simulations. *Phys. Rev. E*, **66**, 056703 (2002).
[14] N.B. Wilding, A.D. Bruce. Density fluctuations and field mixing in the critical fluid. *J. Phys. Condens. Matter*, **4**, 3087 (1992).
[15] N.B. Wilding. Critical-point and coexistence-curve properties of the Lennard-Jones fluid: a finite-size scaling study. *Phys. Rev. E*, **52**, 602 (1995).
[16] N.B. Wilding, K. Binder. Finite-size scaling for near-critical continuum fluids at constant pressure. *Physica A*, **231**, 439 (1996).
[17] M.E. Fisher, G. Orkoulas. The Yang-Yang anomaly in fluid criticality: experiment and scaling theory. *Phys. Rev. Lett.*, **85**, 696 (2000).
[18] G. Orkoulas, M.E. Fisher, A.Z. Panagiotopoulos. Precise simulation of criticality in asymmetric fluids. *Phys. Rev. E*, **63**, 051507 (2001).
[19] M.M. Tsypin, H.W.J. Blote. Probability distribution of the order parameter for the three-dimensional Ising-model universality class: a high-precision Monte Carlo study. *Phys. Rev. E*, **62**, 73 (2000).
[20] R. Hilfer, N. Wilding. Are critical finite-size scaling functions calculable from knowledge of an appropriate critical exponent? *J. Phys. A*, **28**, L281 (1995).
[21] J.P. Valleau. A thermodynamic-scaling study of gibbs-ensemble Monte Carlo. *Mol. Simul*, **29**, 627 (2003).